



HAL
open science

Geochemical identification of potential DNA-hotspots and DNA-infrared fingerprints in lake sediments

Hussein Kanbar, Fredrik Olajos, Göran Englund, Michael Holmboe

► To cite this version:

Hussein Kanbar, Fredrik Olajos, Göran Englund, Michael Holmboe. Geochemical identification of potential DNA-hotspots and DNA-infrared fingerprints in lake sediments. *Applied Geochemistry*, 2020, 122, pp.104728. 10.1016/j.apgeochem.2020.104728 . hal-03035974

HAL Id: hal-03035974

<https://hal.science/hal-03035974>

Submitted on 28 Dec 2022

HAL is a multi-disciplinary open access archive for the deposit and dissemination of scientific research documents, whether they are published or not. The documents may come from teaching and research institutions in France or abroad, or from public or private research centers.

L'archive ouverte pluridisciplinaire **HAL**, est destinée au dépôt et à la diffusion de documents scientifiques de niveau recherche, publiés ou non, émanant des établissements d'enseignement et de recherche français ou étrangers, des laboratoires publics ou privés.



Distributed under a Creative Commons Attribution 4.0 International License



Geochemical identification of potential DNA-hotspots and DNA-infrared fingerprints in lake sediments

Hussein Jaafar Kanbar^{a,*}, Fredrik Olajos^b, Göran Englund^b, Michael Holmboe^{a,**}

^a Department of Chemistry, Umeå University, SE-901 87, Umeå, Sweden

^b Department of Ecology & Environmental Sciences, Umeå University, Umeå, Sweden

ARTICLE INFO

Editorial handling by Prof. M. Kersten

Keywords:

DNA sorption
Sediment grain size
Mineralogy
Clay minerals
Organic matter

ABSTRACT

DNA preserved in sedimentary materials can be used to study past ecosystem changes, such as species' colonization and extinction. It is believed that minerals, especially clay minerals, enhance the preservation of DNA. However, the role of minerals, as well as organic matter, on DNA sorption in heterogeneous sediments is still not clear. In this study, we examined the effect of mineral and organic matter on DNA binding in lake sediments. Bulk and size-fractionated sediments (0–4, 4–16, 16–64, and >64 μm), having different mineral and organic composition, were used to test DNA sorption; similar experiments were also run after the removal of sedimentary organic matter. Additionally, diffuse reflectance infrared spectroscopy (DRIFT) was used to determine the chemical changes caused by DNA sorption and subsequently produce a DNA-infrared (IR) fingerprint. Clay minerals were the main minerals to sorb DNA in the different samples. Moreover, mica promoted DNA sorption in all size fractions, while chlorite promoted DNA sorption in size fractions greater than 16 μm; clay-mineral and organo-mineral complexes caused a preference of certain clay minerals over others. Sedimentary organic matter affected DNA sorption by covering as well as by amplifying potential DNA binding sites, yet DNA sorption did not change significantly. DNA sorption showed IR spectral modifications mainly at ~1640, 1416, and 1231 cm⁻¹. Interestingly, the DNA-IR fingerprint in the heterogeneous sediments was evident by those peaks after spectral subtraction. Finally, we proposed a simple model, based on sediment geochemistry, that can be used to determine potential DNA-hotspots in sediments.

1. Introduction

Sediments and soils can be seen as natural archives that store information about past ecosystem changes. An important information carrier is Deoxyribonucleic acid (DNA). Indeed, DNA can be preserved for tens and hundreds of thousands of years once bound to soils and sediments (e.g., Giguët-Covex et al., 2014; Kisand et al., 2018; Olajos et al., 2018; Slon et al., 2017). However, the amount and quality of DNA that can be extracted from different sedimentary materials are highly variable. Therefore, understanding the conditions that promote DNA sorption and preservation can greatly enhance the utility of this tool to reconstruct ecological communities. A key mechanism for DNA preservation in sediments is absorption onto minerals in general and clay minerals in particular (Levy-Booth et al., 2007; Yu et al., 2013). Thus, there is a need to develop a more detailed understanding of the interactions between DNA and sediment components (minerals and

organic matter). In the recent years, the interaction between nucleotides or DNA and well-defined homo-ionic clay minerals has been studied as a function of pH, ionic strength, pressure, temperature, cation type, cation concentration, contact time, nucleotide length, and others (e.g., Cai et al., 2006a; Freeman et al., 2020; Levy-Booth et al., 2007; Pedreira-Segade et al., 2018; Sheng et al., 2019; Xie et al., 2019; Xue and Feng, 2018; Yu et al., 2013). Clay minerals are ideal candidates for studying DNA-mineral interactions due to their net negative charges and relatively high surface areas. Cation bridges between clay mineral surfaces and phosphate moieties of DNA (or nucleotides) render DNA strands stable against enzymatic degradation (Cai et al., 2006c; Levy-Booth et al., 2007), thus partially explaining DNA preservation for extended periods.

The changes caused by DNA binding onto clay minerals (and other minerals) have been revealed by several tools, including X-ray diffraction (XRD), X-ray absorption spectroscopy (XAS), atomic force

* Corresponding author.

** Corresponding author.

E-mail addresses: hussein.kanbar@umu.se (H.J. Kanbar), michael.holmboe@umu.se (M. Holmboe).

<https://doi.org/10.1016/j.apgeochem.2020.104728>

Received 18 May 2020; Received in revised form 21 July 2020; Accepted 6 August 2020

Available online 18 August 2020

0883-2927/© 2020 The Author(s). Published by Elsevier Ltd. This is an open access article under the CC BY license (<http://creativecommons.org/licenses/by/4.0/>).

microscopy (AFM), and infrared (IR) spectroscopy, such as Fourier transform infrared (Cai et al., 2006; Freeman et al., 2020; Huang et al., 2016; Sheng et al., 2019; Xu, 2010). Among these tools, IR spectroscopy is reliable, fast, and cost-effective. Although IR spectroscopy was successfully used to identify chemical changes after DNA sorption onto pure clay minerals (e.g., Sheng et al., 2019), these changes are not easily detected in heterogeneous materials due to the interference of DNA, mineral, and organic infrared bands.

Sediment coring and sedimentary ancient DNA (sedaDNA) extraction have frequently been used in paleo-ecological studies to explore long term changes in species diversity (e.g., Boere et al., 2011; Huerlimann et al., 2020; Voldstad et al., 2020). Moreover, several studies have reported inconsistencies between sedaDNA and macrofossils within the same medium (Alsos et al., 2018; Clarke et al., 2019a; Giguet-Covex et al., 2019). For example, Pedersen et al. (2013) detected a well-represented taxon by macrofossil, but not by sedaDNA. Multiple non-exclusive explanations were proposed, such as analytical issues, fossilization, extraction methods, and high abundance of some taxa that might overwhelm the rarest ones. Other concerns that might affect sedaDNA records include DNA transfer processes, place and quantity of the produced DNA, polymerase chain reaction (PCR) inhibitors, competition between taxa during PCR, preservation/degradation of sedaDNA, DNA contamination, and completeness of reference databases (e.g., Combs et al., 2015; Deiner et al., 2017; Parducci et al., 2018). Additionally, Huerlimann et al. (2020) raised the concern that clay minerals and organic matter (OM) tightly bind DNA, leading to the failure in detecting some taxa if the DNA extraction methods are not optimized for such samples. Therefore, there is a need for a more detailed understanding of the interactions between DNA and sedimentary components.

In some studies, sedaDNA abundance was linked to the clayey nature of the samples. However, the link was established based on lithostratigraphy and grain size (i.e., the fraction smaller than 2 or 4 μm , which is the clay fraction), but not on individual clay minerals. Other studies found opposite results of DNA preservation with regards to clays and OM; indeed, both positive and negative correlations were established (Alsos et al., 2018; Clarke et al., 2019a; Giguet-Covex et al., 2019; Parducci et al., 2019). The negative correlation between clays and DNA was case-specific and was attributed to the fact that the clayey materials were formed by glaciers and therefore do not hold sedaDNA (Giguet-Covex et al., 2019). Oppositely, the positive correlation was explained by the relatively high surface charges of clay minerals (Levy-Booth et al., 2007). Moreover, DNA might compete with other organic molecules, i. e., OM in general, for mineral binding sites. In lake sediments, however, the interactions between DNA and sediment components are expected to be complex partially due to organo-mineral and mineral-mineral complexes. These notions and others highlight the importance of coupling sediment geochemical characteristics to DNA binding and preservation. To the best of our knowledge, a direct link between DNA sorption and sedimentary components in general and clay minerals in particular has not been established. Therefore, the effects of sediment components on DNA binding were investigated and the consequent chemical changes were identified by IR fingerprints. Finally, a simple model is presented for the identification of possible DNA-hotspots in heterogeneous materials (e.g., soils and sediments), which can facilitate the detection of rare taxa.

2. Materials and methods

2.1. Sedimentary materials

A sediment core was collected from Hotagen, a lake in west-central Sweden, using an 86-mm inner diameter piston corer (Olajos et al., 2018). A sediment sample was collected every 5 cm along the 2.3-m core. Each of the 45 samples was divided into two parts: an intact part (named bulk) and a size-fractionated part of particle sizes 0–4, 4–16,

16–64, and >64 μm ; size-fractionation was done according to Stokes' law (Bergaya and Lagaly, 2013). To avoid physical or chemical modifications that possibly damage stored DNA (e.g., sedaDNA) and to maintain the characteristics of sedimentary particles, the samples were not disaggregated. It was therefore assumed that sedimentary mineral-mineral and organo-mineral complexes remained mostly intact. In another study, the physical, physico-chemical, chemical, organic, and mineral properties of the sediments showed distinct features with depth; accordingly, a clear distinction was made between two units (Kanbar et al., in preparation). The deepest unit (U2: 200–225 cm) marked the transition from the Late Pleistocene to the Holocene (10,000–8000 BP), as indicated by drastic mineralogical changes. These sediments were relatively poor in organic matter ($15 \pm 9\%$) and clay minerals (chlorite and mica, $34 \pm 7\%$), and rich in quartz and feldspars ($56 \pm 5\%$); feldspars is the sum of albite and K-feldspars. The deepest sediment (225 cm) was identified as glacial till (named till). The more shallow and recent unit (U1: 0–195 cm) only showed minor weathering attributes that were noticeable at a chemical level, but not on a mineralogical one (8000 BP to present). These sediments were relatively rich in organic matter ($27 \pm 2\%$) and clay minerals ($49 \pm 5\%$).

2.2. X-ray diffraction

The crystalline minerals of the bulk and size-fractionated sediments were determined by powder X-ray diffraction (XRD) measurements using PANalytical X'pert³ powder diffractometer ($\text{CuK}\alpha$ radiation 1.54187 Å). The minerals were identified by the Crystallography Open Database (COD) and quantified by the Rietveld refinement method using the GUI Profex-BGMN (Doebelin and Kleeberg, 2015; Post and Bish, 1989). The fundamental parameters approach (FPA) was set to match the instrument's settings (e.g., divergence slits, soller slits, and optical elements in the beam path) for accurate peak shape modeling. The experimental diffractograms were fitted to the mineral phases detected in the sediments. The quality of the fit was assessed by goodness-of-fit (GoF) and chi-squared values (χ^2). It should be noted that only the crystalline minerals are reported in this study; amorphous phases, allophanes, and poorly crystalline minerals were not taken into consideration.

2.3. Grain size distribution

The grain size distribution (GSD) of non-freeze-dried bulk samples was determined by laser diffraction (Partica LA-950V2 Laser Scattering Particle Size Distribution Analyzer from Horiba). The samples were agitated in a sample bath with distilled water and grain size measurements were done before and after 1-min sonication. Sonication is expected to break sedimentary aggregates (e.g., mineral-mineral and organo-mineral complexes). The volumetric percentages were used to calculate the percentiles D_{16} , D_{50} , and D_{90} (in μm).

2.4. DNA sorption onto sediments

Low molecular weight salmon sperm DNA was purchased from Sigma Aldrich (CAS 100403-24-5). DNA sorption experiments were carried out on bulk and size-fractionated sediments (named Sed). DNA sorption experiments were also done on the same sediments after OM removal (named $\text{Sed}_{\text{inorg}}$) by sodium hypochlorite (e.g., Anderson, 1961; Mikutta et al., 2005); detailed information about OM removal by NaOCl is included elsewhere (Margenot et al. (2019) and Appendix A1). Briefly, 8 mg of sediments (Sed and $\text{Sed}_{\text{inorg}}$) were mixed in 2 ml solutions containing 200 $\mu\text{g}/\text{ml}$ DNA, 10 mM Tris base buffer (trisaminomethane), and 25 mM CaCl_2 for 2 h; detailed information is included in Appendix A2. The remaining DNA concentrations were used to calculate the sorbed DNA amounts; dissolved DNA was quantified by a UV-Vis spectrophotometer based on the absorbance at 260 nm (Lambda 750 UV/Vis/NIR spectrometer by PerkinElmer). The DNA contents sorbed

onto Sed and Sed_{inorg} are named DNA_s and DNA_{s-inorg}, respectively. DNA sorption experiments were run as triplicates (named -DNA). Additionally, control treatments, named -Ctr, were run along with the samples; the controls included sediments with Tris and CaCl₂ solutions, but not DNA. After the DNA sorption experiment, the -DNA and -Ctr treated sediments were freeze-dried before infrared analyses. The experimental conditions are based on similar DNA sorption experiments (e.g., Cai et al., 2006b; Pedreira-Segade et al., 2018). It should be noted that the sorbed DNA contents reported here depend on the experimental conditions; therefore, they do not reflect sedaDNA contents. The objective of the sorption experiment is to find a link between DNA sorption and sedimentary components (minerals and organic matter) and consequently to locate preferential DNA sorption sites in lake sediments (i.e., DNA-hotspot).

2.5. Diffuse reflectance infrared fourier transform

Diffuse reflectance infrared Fourier transform spectra (DRIFT; IFS 66v/s by Bruker) were collected for the initial (-initial), control (-Ctr), and DNA treated samples (-DNA). The dried samples were homogenized with KBr. For each sample, 128 spectra were recorded under vacuum (<7 mbar) in the 5200 and 400 cm⁻¹ range with 4 cm⁻¹ spectral resolution. The raw DRIFT spectra were treated using the open-source MCRALS GUI provided by the Vibration Spectroscopy Core Facility at Umeå University (www.umu.se/en/research/infrastructure/visp/downloads/). This script was designed for biological material, however, it can identify, characterize, and categorize chemical composition (Felten et al., 2019, 2015), thus making the script applicable to the initial, -Ctr, and -DNA treated Sed and Sed_{inorg} samples. The organic matter contents reported hereafter are based on organic IR signatures (e.g., Rosén et al., 2010; Vogel et al., 2008). The DNA-IR fingerprint of the sorbed DNA onto the sediments was determined by subtracting the Sed-Ctr from Sed-DNA IR spectra after spectral normalization (detailed information is included in Appendix A3). The DNA-IR fingerprint was then compared to that of the salmon sperm DNA that was treated with 25 mM CaCl₂ and 10 mM Tris.

3. Results

3.1. DNA sorption onto bulk sediments

DNA sorption (DNA_s) onto the bulk U1 samples ranged between 15 and 19 µg/mg (Fig. 1a). The DNA_s values were relatively lower in the U2

sediments, especially in the till (same as 225 cm, ~2 µg/mg). Quartz and feldspars (albite + K-feldspars) were the predominant minerals of the till (68%), clay minerals (Σclays: chlorite + mica) represented a small fraction (18%), and OM was very low (~0.27%) (Fig. 1b). Quartz and feldspars have significantly lower surface areas and surface charges compared to clay minerals (e.g., Yu et al., 2013 and references therein), which explain relatively low DNA_s in the till and other U2 sediments. Oppositely, the higher clay mineral and OM contents in the upper U2 sediments and all U1 sediments explain relatively higher DNA_s. The role of minerals and OM on DNA sorption is highlighted by considerable differences in DNA_s between U1 and U2 sediments. The DNA_s of the 205-, 210-, 215-, and 225-cm sediments were 17 ± 5%, 25 ± 4%, 35 ± 4%, and 86 ± 1% lower than the average DNA_s in the U1 sediments. In sediments and soils having pH greater than 5 (case of the initial Hotagen sediments), cation-bridge formation is expected to be the predominant mechanism for DNA binding. The cation bridge is formed between the phosphate moieties of DNA and the negatively charged oxide surfaces of minerals and OM (Levy-Booth et al., 2007; Sheng et al., 2019). However, OM (e.g., humic substances) also bind onto mineral oxide surfaces. Therefore, competition between OM and DNA might reduce DNA sorption onto minerals. The 1- and 165-cm sediments showed slightly higher DNA_s than the other U1 sediments. This might be caused by higher clay mineral and OM contents in the 1-cm sediment. As for the 165-cm sediment, it showed bigger aggregates than the other samples, as indicated by a relatively higher difference in percentiles before and after sonication (Fig. 1c). This difference points to possible DNA binding sites that can become exposed upon disaggregation. Accordingly, aggregate type (organo-mineral and mineral-mineral complexes) and sediment size are expected to play a role in DNA binding. So, even with similar sediment mineralogy, different DNA_s might result based on aggregate characteristics and available DNA binding sites. This was more obvious in OM-rich samples since OM acts as a cementing factor in organo-mineral complexes. The role of OM in aggregate size was seen by the relatively higher difference in percentiles after sonication in the OM-rich samples of U1 (Fig. 1c).

3.2. Sedimentary organic matter plays a role in DNA sorption but not in terms of quantity

The DNA_s and DNA_{s-inorg} showed similar trends as a function of depth, mainly noticeable in the U1–U2 transition (Fig. 1a). Interestingly, unlike DNA_s, the DNA_{s-inorg} of the 165-cm sediment was similar to the surrounding sediments. On the one hand, OM that is bound to minerals

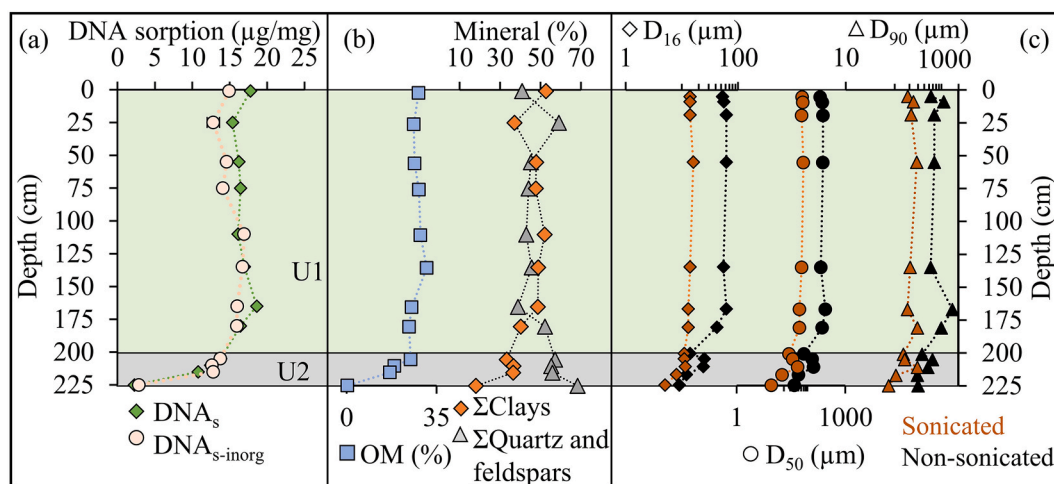


Fig. 1. Variation of a) DNA_s (DNA sorption onto sediments) and DNA_{s-inorg} (DNA sorption onto Sed_{inorg}, i.e., sediments without organic matter), b) organic matter (OM) and minerals (Σclays and Σquartz and feldspars), and c) percentiles (D₁₆, D₅₀, and D₉₀) of bulk sediments as a function of depth. The symbols of DNA_s and DNA_{s-inorg} represent average values (n = 3).

(mainly clay minerals) occupies possible DNA binding sites, thus reducing the DNA binding capacity (Cai et al., 2006b; Crecchio et al., 2005). On the other hand, surface charges of OM might increase DNA binding capacity (Pietramellara et al., 2009; Xue and Feng, 2018). The mineralogy, organic composition, and aggregates dictate which of these two processes predominates in lake sediments.

In the Hotagen sediments, $DNA_{s-inorg}$ showed to be lower, equal, or higher than DNA_s , depending on sediment composition (i.e., sediment depth and size fraction). The first case applied to the 1-75-cm sediments which contained comparable amounts of clay minerals and OM throughout most U1 sediments (Fig. 1a and b). Furthermore, after OM removal, which caused the disaggregation of organo-mineral complexes, more mineral surfaces were exposed. These surfaces had less significant DNA sorption than those offered by OM, indicating that OM promoted DNA binding in these sediments. In most sediments below 75 cm, OM removal did not affect DNA_s , indicating that the two processes mentioned above (mineral surface exposure and OM removal) had neutralizing effects on DNA sorption. Moreover, the similarity in DNA_s and $DNA_{s-inorg}$ in the U2 sediments is further linked to the significantly low OM contents and consequently insignificant organo-mineral complexes (Fig. 1b and c). The third case ($DNA_{s-inorg} > DNA_s$) was only and slightly seen in the 215-cm sediment (more examples are given in the next section). Although the difference might be insignificant, higher $DNA_{s-inorg}$ could come from the disaggregation of organo-mineral complexes; the newly exposed DNA binding sites of the minerals overcompensated those of OM or organo-mineral complexes. Additionally, the deepest U2 sediment contained insignificant amounts of OM, making clay minerals the main aggregating factor. Therefore, higher $DNA_{s-inorg}$ might be linked to the disaggregation of mineral-mineral complexes,

consequently leading to more DNA binding sites. Finally, the role of OM in DNA sorption was sample-specific in the Hotagen sediments, yet the change in DNA sorption quantity might be insignificant.

3.3. Role of sediment geochemistry on DNA sorption

The 0-4- μ m size fractions had the highest DNA_s , followed by 4-16, 16-64, and >64 μ m (Fig. 2). The same applied to the clay mineral contents (Σ clays), suggesting the role of clays in increasing DNA_s due to their high surface areas (Levy-Booth et al., 2007; Yu et al., 2013). A more direct comparison of DNA_s , $DNA_{s-inorg}$, and minerals in the different size fractions is presented in Fig. A1 (Appendix). Moreover, the general trend of DNA_s in the sediment depths, i.e., higher values in U1 in comparison to U2, was seen for all the size fractions. Interestingly, the three fractions (4-16, 16-64, and >64 μ m) of the 1-, 135-, and 165-cm sediments showed similar DNA_s (16.6 ± 1.2 , 17.6 ± 0.7 , and 18.6 ± 0.3 μ g/mg, respectively), while DNA_s of the 0-4- μ m fractions were higher (22.8, 21.3, and 21.9 μ g/mg, respectively). The geochemical distinction between the 0-4 μ m and the coarser fractions was established by multivariate curve resolution alternating least square - MCR-ALS (Kanbar et al., in preparation). In all cases, DNA_s was linked to the sum of clay minerals in general for all size fractions (Fig. 2a-d); yet, it was most obvious in the 0-4- μ m size fraction (Fig. 2a). In addition to clay minerals, DNA_s can also be indirectly linked to quartz and feldspars. This was seen by the opposite trends between quartz and feldspars on the one hand and DNA_s on the other (e.g., the 4-16-, 16-64-, and >64- μ m size fractions, Fig. 2b-d).

The main variation between DNA_s and $DNA_{s-inorg}$ occurred in the U1 sediments, while it was quasi-absent or significantly reduced in U2

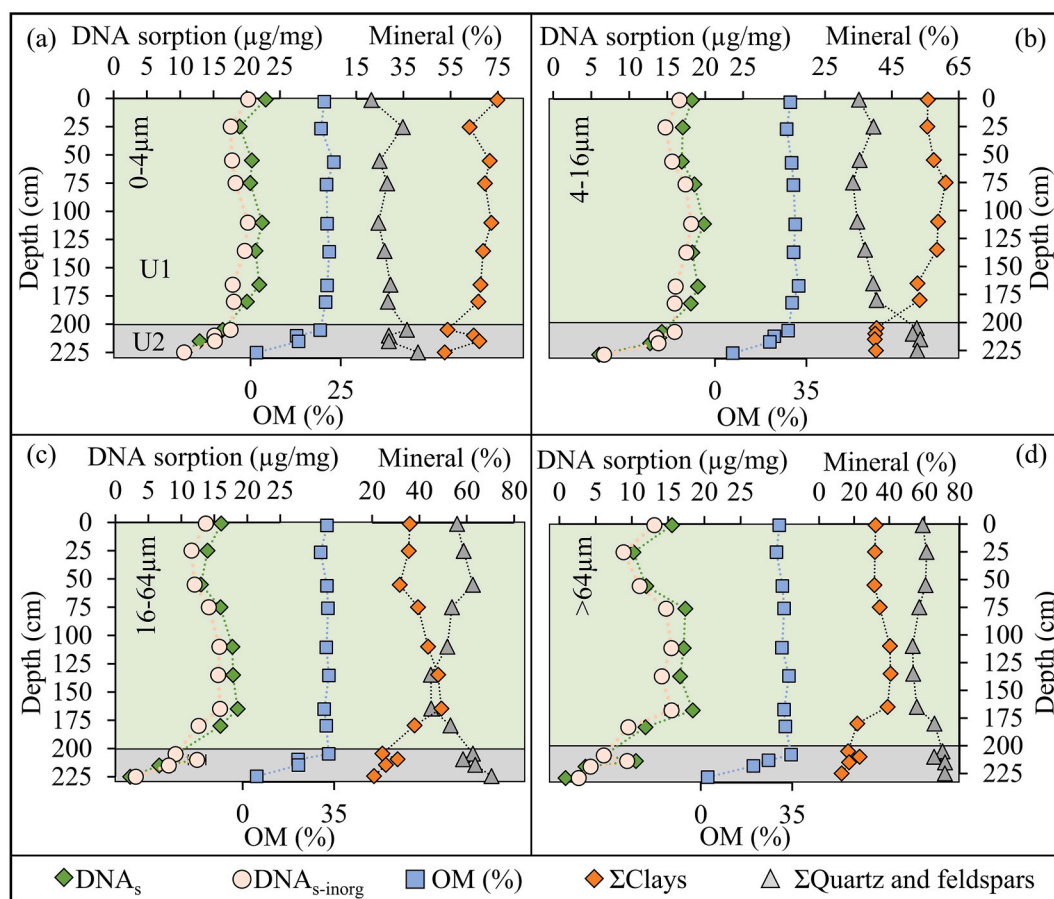


Fig. 2. Variation of DNA_s (DNA sorption onto sediments), $DNA_{s-inorg}$ (DNA sorption onto Sed_{inorg} , i.e., sediments without organic matter), organic matter (OM), and minerals (Σ clays and Σ quartz and feldspars) for a) 0-4- μ m, b) 4-16- μ m, c) 16-64- μ m, and d) > 64- μ m size fractions as a function of sediment depth. The symbols of DNA_s and $DNA_{s-inorg}$ represent average values ($n = 3$).

(Fig. 2). The $\text{DNA}_{\text{s-inorg}}$ of some U2 sediments, e.g., the 0-4- μm fractions of 205 and 215 cm, were higher than DNA_{s} . In these relatively OM-poor sediments, the mineral surfaces that protruded after disaggregation could compensate the OM surfaces (as discussed in Section 3.2). In this case, OM had a less significant role in DNA sorption than the aggregates. However, the $\text{DNA}_{\text{s-inorg}}$ in almost all size fractions of the U1 sediments were lower than DNA_{s} , indicating the role of OM in promoting DNA sorption.

3.4. Changes in sediment IR characteristics after DNA sorption

The geochemical characteristics of the sediments showed major differences in the IR spectra between sediment sizes lower and greater than 4 μm (Kanbar et al., in preparation). The IR modifications caused by DNA binding onto bulk sediments were based on 2 steps. The first step indicated Ca binding onto mineral or organic surfaces (case of the control samples, -Ctr). The second step indicated the sorption of DNA

most probably by cation-bridge formation between surface-bound Ca and DNA (case of DNA-treated samples; -DNA). Therefore, the IR spectra are compared between initial, -Ctr, and -DNA samples. The main IR alterations occurred in the 1750-1300 cm^{-1} and 3700-2800 cm^{-1} regions, while apparently insignificant changes occurred in the 1300-900 cm^{-1} region (Fig. 3a and b). Organic matter, including DNA, and cations form stable complexes via O-containing functional groups, such as $-\text{COOH}$ ($\sim 1600 \text{ cm}^{-1}$) and $-\text{OH}$ ($\sim 3400 \text{ cm}^{-1}$) (Drever and Vance, 1994; Franchi et al., 1999; Huang et al., 2016). The major IR characteristics of the salmon sperm DNA, as identified in this study, and according to Huang et al. (2016) and Han et al. (2018), were the phosphate backbone of DNA (P=O stretching and O-P-O bending at 1055 and 1231 cm^{-1} , respectively), C=C and C=O stretching of the amine bases at 1600-1400 cm^{-1} and 1690-1660 cm^{-1} , respectively, CH_2 stretching at 2890 and 2940 cm^{-1} , and the OH and NH stretching vibrations in the 3400-3000 cm^{-1} region (Fig. 3c).

The phosphate backbone IR peaks of the salmon sperm DNA (1055

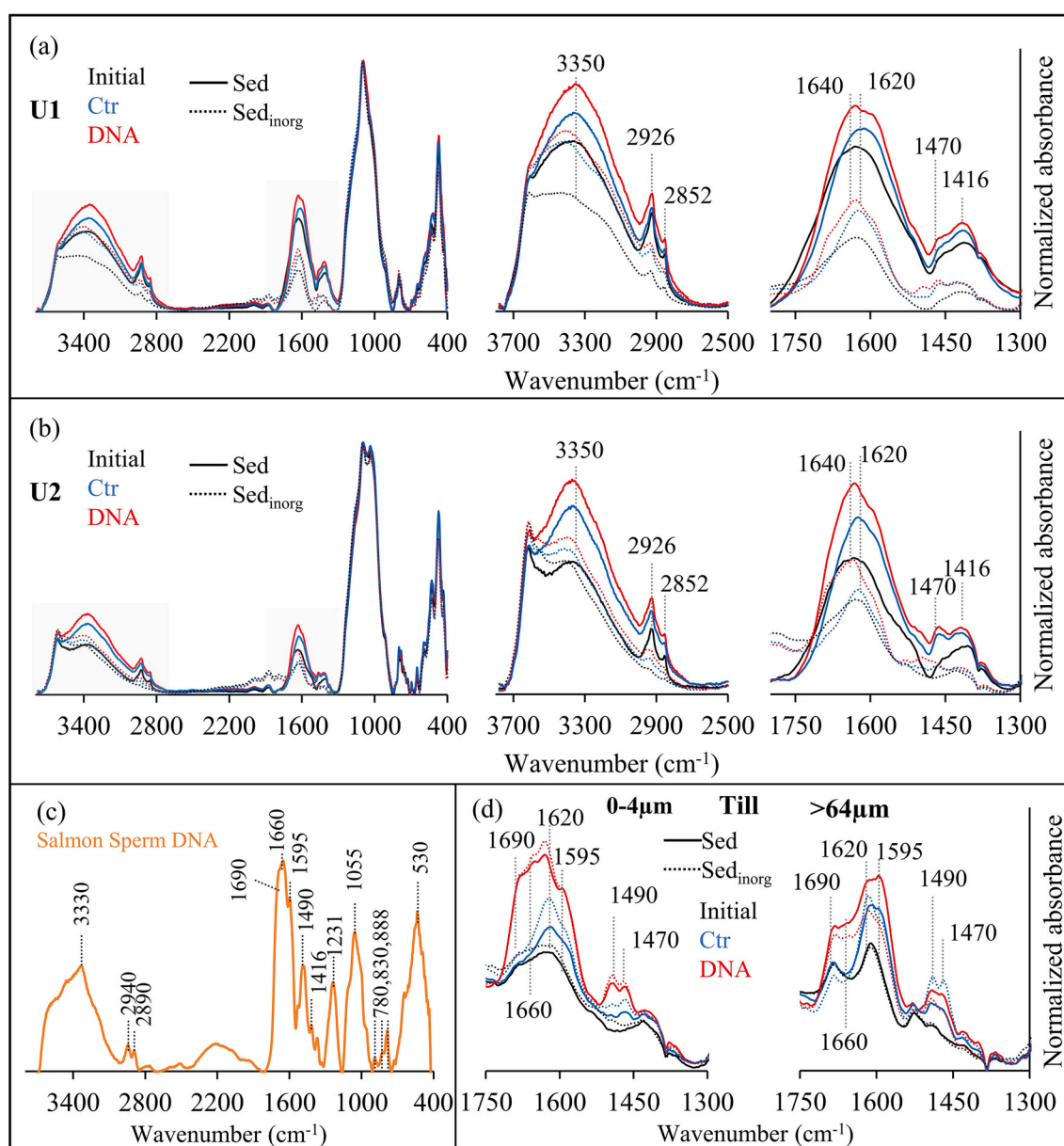


Fig. 3. DRIFT spectra of the initial (black), control (blue), and DNA (red) treated bulk samples (Sed and $\text{Sed}_{\text{inorg}}$) for a) U1, b) U2, and d) the till. c) The DRIFT spectrum of the salmon sperm DNA. Regions of interests (in a and b) are highlighted in grey color. (For interpretation of the references to color in this figure legend, the reader is referred to the Web version of this article.)

and 1231 cm^{-1}) coincide with the Si–O stretching bands of quartz, feldspars, and clay minerals in the $1250\text{--}950\text{ cm}^{-1}$ region (Fig. 3a–c). Therefore, these main DNA-IR signatures could hardly be detected in the Hotagen sediments. This would be the case of clay-, quartz-, and feldspar-rich media, i.e., most soils and sediments. However, there was a slight protrusion of a shoulder at $1300\text{--}1150\text{ cm}^{-1}$ for DNA treated samples. The amine characteristic bands of DNA (in the 1690 and $1470\text{--}1400\text{ cm}^{-1}$ regions) overlap with organic matter bands (–C–O stretching vibration of carboxyl groups of humic substances) and water bending bands (Rosén et al., 2010). Nonetheless, these peaks, roughly centered at 1620 , 1470 , and 1416 cm^{-1} , increased in the control samples due to the –OH and amine bands of Tris (Fig. A2, Appendix), and further increased

after DNA sorption due to nucleobase bands (Banyay et al., 2003). However, there was no link between peak intensity or area and the amount of DNA sorbed.

In addition to the vertical shifts, a more notable horizontal shift of the water bending peak occurred from ~ 1640 to 1615 cm^{-1} upon surface Ca binding (–Ctr); this peak then shifted to 1640 cm^{-1} after DNA sorption (Fig. 3a and b). This change indicates the sorption of surface Ca followed by cation-bridge formation (DNA binding). These horizontal displacements occurred in Sed and Sed_{inorg}, yet they were more noticeable in Sed_{inorg} due to narrower 1630 cm^{-1} bands (Fig. 3a and b). As for the till, the IR spectra (bulk and fractions) were unique due to quartz and feldspar abundance and clay mineral and organic matter

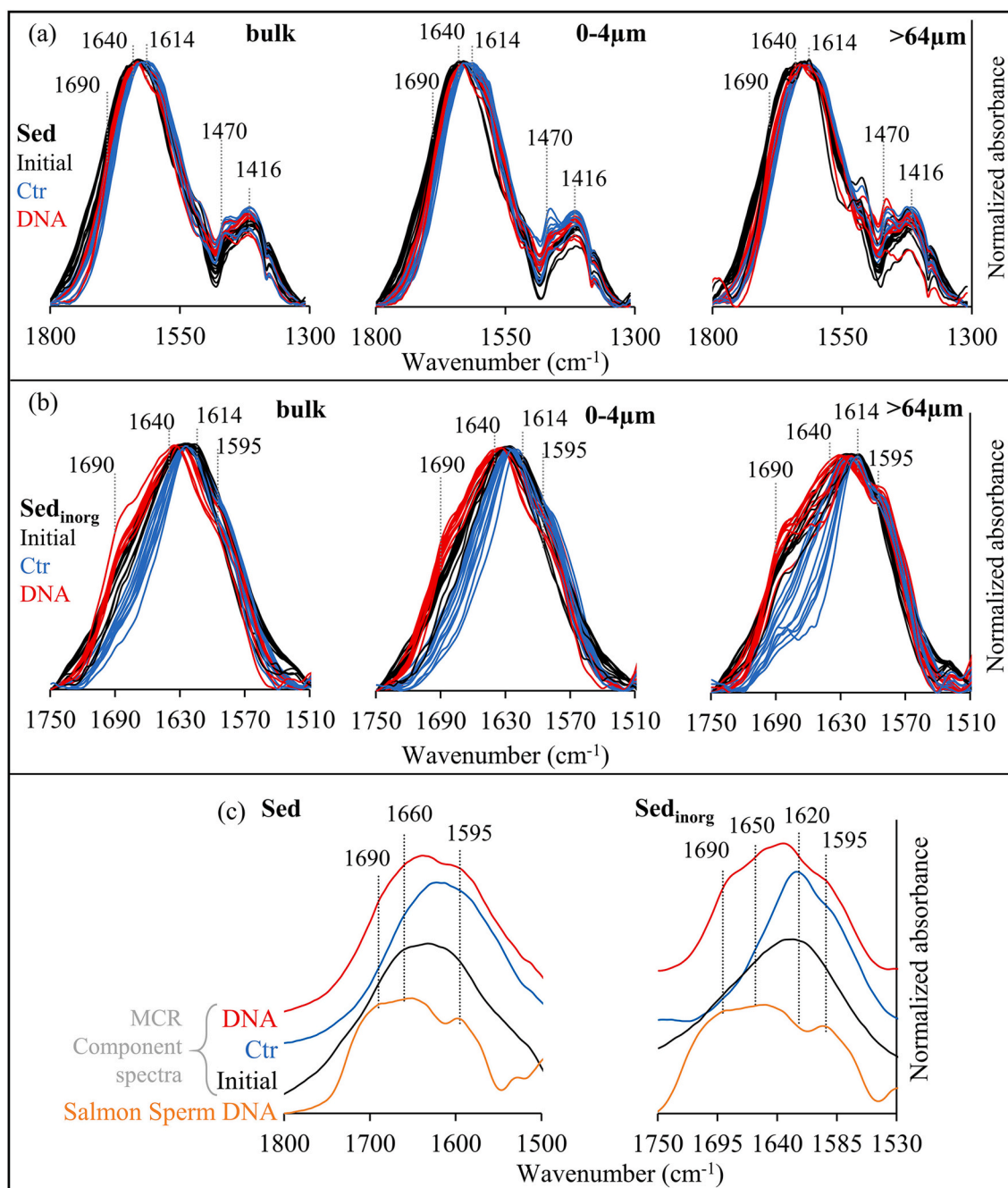


Fig. 4. a-b) Compiled DRIFT spectra showing the change in the $\sim 1600\text{ cm}^{-1}$ region of the initial (black), control (blue), and DNA (red) treated sediments. The change is shown for a) Sed and b) Sed_{inorg} samples and for bulk, 0–4- μm , and >64- μm size fractions. c) The component spectra produced by the multivariate statistical analysis (MCR-ALS) of the initial, Ctr, and DNA treated samples for Sed and Sed_{inorg}. Salmon sperm DNA spectra are included for comparison. (For interpretation of the references to color in this figure legend, the reader is referred to the Web version of this article.)

scarcity. As a result, the DNA-IR characteristic bands at 1690 and 1660 cm^{-1} were obvious for all fractions, especially for the 0-4- μm size fraction (Fig. 3d). Finally, the 2926 and 2852 cm^{-1} peaks (C–H stretching of OM) increased in -Ctr and -DNA samples. The same applied for the 3600-3000 cm^{-1} band (Fig. 3a and b). These variations cannot be linked to DNA sorption as the change in the peak intensities was not consistent between the initial, -Ctr, and -DNA samples.

The IR spectra of the initial, -Ctr, and -DNA treated sediment fractions showed a change in the 1690-1600 cm^{-1} region (Fig. 4a and b). Even though the 0-4- μm fractions had higher DNA_s than the coarser fractions (especially >64- μm fractions), the DNA-induced IR change was similar for the different size fractions (Fig. 4a). The DNA-induced IR change was clearer in $\text{Sed}_{\text{inorg}}$ due to the absence of overlapping OM-IR peaks (Fig. 4b). Furthermore, multivariate statistical analysis (MCR-ALS) produced three resolved component spectra that represent the initial, -Ctr, and -DNA treated samples (Fig. 4c). The DNA component spectra showed some characteristics of the salmon sperm DNA used in this study, as indicated by peaks or shoulders in the 1690-1595 cm^{-1} region (Fig. 4c).

4. Discussion

4.1. The significance of clay minerals on DNA sorption in lake sediments

The significance of pure and homo-ionic clay minerals on DNA sorption has been presented in the literature (e.g., Benetoli et al., 2008; Franchi et al., 1999; Pedreira-Segade et al., 2018). However, this significance is expected to be different in real lake sediments due to the presence of clay-mineral and organo-mineral complexes. In sediments and soils, clay minerals are not limited to clay fractions (i.e., the fraction <2 or 4 μm) since they are parts of bigger aggregates (clay-mineral and organo-clay); this was the case of the Hotagen sediments (Fig. A1, Appendix). However, the correlation between DNA sorption (DNA_s and $\text{DNA}_{s\text{-inorg}}$) and the sum of clay minerals (Σclays) was not dependent on particle size, rather it was significant regardless of size (Fig. 5a, P values and correlation coefficients are included in Appendix A4); clay minerals showed a higher correlation with $\text{DNA}_{s\text{-inorg}}$ in comparison to DNA_s . This higher correlation is due to the disaggregation of organo-mineral complexes, thus creating more available clay mineral surfaces. Moreover, the correlation was further distinct for individual clay minerals, i.e., for each of chlorite and mica; chlorite was only significantly correlated to DNA_s in size fractions greater than 16 μm (Fig. 5b, correlation coefficients and P values are included in Appendix A5). Even more, the

correlation between chlorite and DNA_s was negative for the 0-4- and 4-16- μm size fractions. This neither indicates that chlorite reduced DNA sorption nor that DNA was not sorbed onto chlorite minerals (as indicated by insignificant correlations, Appendix A5). Rather, the negative correlation might arise from unavailable DNA binding sites caused by organo-mineral or mineral-mineral complexes. Mica, on the other hand, showed to be strongly correlated to DNA_s in all size fractions (Fig. 5b and A5). This shows that mica, which had relatively higher contents in the Hotagen sediments and higher surface charge than chlorite, had the most significant DNA binding sites. Among the discussed minerals in this study, mica minerals generally have the highest surface area, followed by chlorite minerals, feldspar minerals, and finally quartz (Pansu and Gautheyrou, 2006). Quartz and feldspars were negatively correlated to DNA_s (Fig. 5b and A5). Yet, they were indirectly linked to DNA_s by diluting clay minerals in the sediments, consequently reducing DNA_s . This highlights the role of minerals in general, and clay minerals in particular, on DNA sorption. Regardless of the individual clay mineral, it is safe to say that DNA is preferentially stored in clay mineral-rich fine fractions of sediments, as shown by significant correlations between the sum of clay minerals and DNA_s (Fig. 5b and A5); the same applies to OM.

4.2. A simple and inexpensive method to determine DNA-hotspots using sediment geochemistry

The theoretical DNA_s was estimated by multiple linear regression based on only clay minerals (chlorite and mica), all minerals (clay minerals, quartz, and feldspars), clay minerals and organic matter, and all minerals and organic matter as explanatory variables (Fig. 6). The regression statistics, including coefficients and F significance, are included in Appendix A6. The theoretical DNA_s showed a strong correlation to the experimental DNA_s even when only the clay minerals were used as explanatory variables ($R^2 = 0.66$, Fig. 6a). Indeed, clay minerals are the preferential DNA sorbing minerals (Levy-Booth et al., 2007; Yu et al., 2013). The regression slightly increased when quartz and feldspars were added as explanatory variables ($R^2 = 0.69$, Fig. 6b). Interestingly, when OM and the clay minerals were taken as explanatory variables in the multiple regression analysis, the correlation became higher ($R^2 = 0.91$, Fig. 6c). However, the best fit resulted when all minerals, regardless of their direct link to DNA sorption, and OM were included in the multiple regression analysis ($R^2 = 0.92$, Fig. 6d). This fit between the experimental and theoretical DNA_s highlights the role of sediment geochemistry on DNA sorption. The significance of clay minerals on DNA sorption is not straightforward, partially due to the

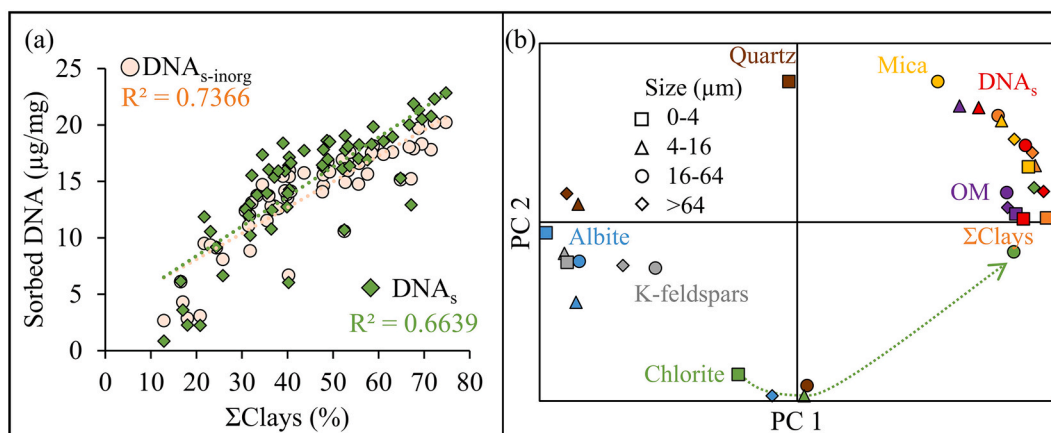


Fig. 5. a) The sorption of DNA onto Sed (DNA_s) and $\text{Sed}_{\text{inorg}}$ ($\text{DNA}_{s\text{-inorg}}$), in $\mu\text{g}/\text{mg}$, according to the sum of clay minerals (ΣClays : chlorite + mica); $n = 60$ for each of DNA_s and $\text{DNA}_{s\text{-inorg}}$. b) The principal component analysis (PCA) correlation matrix showing the link between individual minerals (quartz, albitite, K-feldspars, chlorite, and mica), ΣClays , OM, and DNA_s based on sediment size. Each color represents a variable (mineral, OM, or DNA_s) and each shape represents a size fraction. For better visualization of the variation, the four PCA plots (one plot for each size fraction) are merged. The statistical data are found in Appendix A5. (For interpretation of the references to color in this figure legend, the reader is referred to the Web version of this article.)

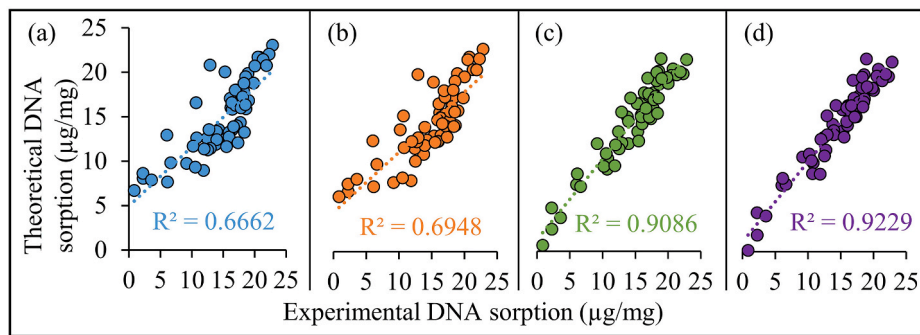


Fig. 6. Multiple linear regression showing the correlation between the theoretical and experimental DNA_s by taking into consideration a) only the clay minerals (i.e., chlorite and mica), b) all minerals (the clay minerals, quartz, and feldspars), c) the clay minerals and organic matter, and d) all the minerals and organic matter as explanatory variables. $n = 60$ for each plot. The regression statistics are included in [Appendix A6](#).

presence of clay-mineral and clay-OM aggregates. Therefore, although not directly linked, OM and minerals, such as quartz and feldspars in this case, have a considerable role in determining sedaDNA-hotspots. Even though the correlations presented here are significant ([Appendix A6](#)), they are solely based on the crystalline minerals and organic matter. Poorly crystalline and amorphous minerals (e.g., ferrihydrite and allophanes) also bind DNA (e.g., [Huang et al., 2016](#); [Saeki et al., 2011, 2010](#); [Schmidt and Martínez, 2017](#)). The importance of such information when identifying potential sedaDNA-hotspots is yet to be explored. Additionally, it must be noted that the multiple regression model is based on internal validations; external validation is needed to evaluate the generality of the model. The purpose of the correlations or the model is not to estimate DNA_s in sediments; the DNA_s and theoretical DNA_s indicated in this study depend on the nature of DNA, experimental conditions, and physico-chemical parameters (e.g., pH and ionic strength), which are expected to differ from in-situ conditions. Rather, the aim is to show the importance of sediment geochemistry when addressing sedaDNA. Indeed, similar approaches can be applied to geochemically heterogeneous sediments and soils to identify possible DNA-hotspots. Therefore, geochemical identification of matrices (soils or sediments) is a fast, cost-effective, and fruitful tool to identify potential DNA-hotspots. Focusing sampling and analysis on such hotspots will provide considerably increased detection probability for rare taxa. However, the limitations and biases resulting from using DNA-hotspots, i.e., clay fractions or clay mineral-rich fractions, in metabarcoding (e.g., over-representation of the rare taxa) must be well identified and overcome before implementing such strategies (e.g., [Giguët-Covex et al., 2019](#)).

4.3. Are we looking at the right place for comprehensive DNA detection?

Recent studies have debated how well sedaDNA abundances represent the occurrence of species (e.g., [Alsos et al., 2018](#); [Clarke et al., 2019a](#); [Giguët-Covex et al., 2019](#); [Parducci et al., 2017](#)). For example, taxa growing merely a few meters from the sampling sites could not be identified even by metagenomic shotgun sequencing ([Parducci et al., 2019](#)). However, in those studies, the abundance of sedaDNA was linked to clay fractions (i.e., the particle sizes below 2 or 4 μm , but not clay minerals). The role of clay fractions and OM in affecting sedaDNA sorption has been reported ([Clarke et al., 2019b](#); [Parducci et al., 2019, 2017](#); [Torti et al., 2015](#)). In this study, the importance of sediment geochemistry in general, and clay minerals in particular, on DNA sorption was seen by significant DNA_s variation between U1 and U2 sediments ([Figs. 1 and 2](#)). This significant mineral variation, i.e., clay minerals, quartz, and feldspars, must be taken into consideration when comparing taxa abundance or concentrations (e.g., via number of reads or positive PCR replicates in metabarcoding). Consequently, and according to the current knowledge about preferential DNA sorption onto clay minerals, the conventional ways of DNA extraction from bulk

samples need to be revisited. More attention should be paid to selective DNA extraction mainly based on mineralogy. Indeed, new or updated sampling designs have been suggested mainly due to the tight binding of DNA onto clay minerals ([Huerlimann et al., 2020](#)). The effect of minerals on DNA binding is most critical in studies where the target taxa are represented by low sedaDNA abundance. Likewise, the mineralogy may be of less concern for taxa with high sedaDNA abundance. The concern of over and under-representation of taxa in one matrix might not be critical, however, it is critical when taxa between different macro-environments are compared, e.g., different layers of lake sediments having mineral variations (e.g., [Giguët-Covex et al., 2019](#)). It should be noted that the correlation between sedaDNA and clay minerals is valid when clay minerals originate from lands or soils where DNA is expected to sorb. On the other hand, if clay minerals originate from other sources, e.g., glacier flours ([Giguët-Covex et al., 2019](#)), then sedaDNA is not expected to be present, which makes the model presented here inapplicable.

4.4. Unveiling the DNA-infrared fingerprint in sediments

Clay minerals and DNA have IR bands in common regions, such as the 1100–950 cm^{-1} region that includes the phosphate moiety of DNA and the Si–O stretching of clay and silicate minerals and the 1690–1614 cm^{-1} region that includes the DNA amine bases (C=C and C=O) and the water bending band in clay minerals. The DNA-IR bands in pure clay mineral-DNA systems can generally be seen without significant IR treatment (e.g., [Benetoli et al., 2008](#); [Cai et al., 2006c](#); [Franchi et al., 1999](#); [Huang et al., 2016](#); [Sheng et al., 2019](#)). In lake sediments, as well as in soils, the detection of DNA related IR peaks is more challenging due to the presence of a combination of interfering mineral and organic matter IR bands, especially in the 530, 1490, 1690, 2900, and 3330 cm^{-1} regions. These challenges were greatly overcome in the Hotagen sediments by IR spectral subtraction. Interestingly, the DNA-infrared fingerprint produced from the heterogeneous sediments resembled the salmon sperm DNA spectrum ([Fig. 7](#)). The most distinct DNA-IR fingerprint was detected by the amine base peaks at 1690, 1660, and 1595 cm^{-1} . The 1690 cm^{-1} peak was more centered (narrow) in Sed_{inorg} due to the absence of overlapping OM IR peaks and for the 0–4- μm size fractions due to low OM contents ([Fig. 7b](#)). Another distinct feature of the DNA-IR fingerprint was the phosphate band at 1231 cm^{-1} . As mentioned earlier, the 1231 cm^{-1} peak interferes with the Si–O stretching bands of clay minerals (1095 cm^{-1}) and quartz or feldspars (1020 cm^{-1}). The 1231 cm^{-1} peak was more noticeable in the quartz- and feldspar-rich >64- μm size fractions since Si–O interferences of these minerals were less intrusive than those of clays. Similarly, the DNA-IR shoulder at 1120 cm^{-1} was mainly detected in the DNA-IR fingerprint spectra of the 0–4- μm size fractions. Even though overlapping with the Si–O stretching band, the DNA-IR peak at 1055 cm^{-1} was occasionally detected in the DNA-IR fingerprint spectra. The DNA-IR fingerprint

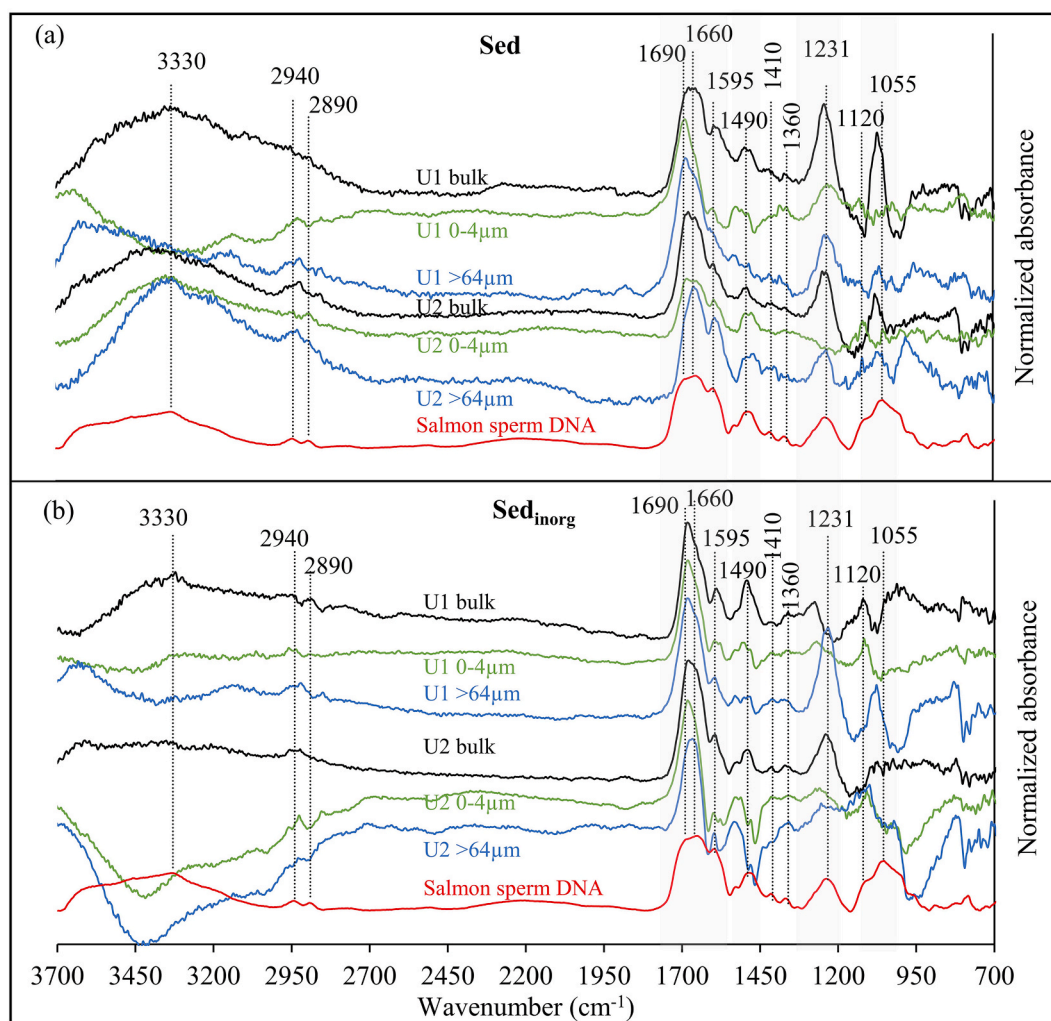


Fig. 7. DNA-IR fingerprint (DRIFT) spectra for a) Sed and b) Sed_{inorg} samples obtained after spectral subtraction (difference between -DNA and -ctr spectra). The IR fingerprint spectra for U1 and U2 samples and for bulk, 0-4- μm , and >64- μm size fractions are included. Regions of interest are highlighted in grey color. Salmon sperm DNA spectra are included for comparison. (For interpretation of the references to color in this figure legend, the reader is referred to the Web version of this article.)

spectra also evidenced the C=C amine stretching peaks of the salmon sperm DNA between 1490 and 1410 cm^{-1} . These peaks could not be evidenced before IR spectral subtraction (Fig. 3). Less significant DNA-IR fingerprints were detected at 2940 cm^{-1} (CH_2 stretching of nucleotides) and 2890 cm^{-1} . These fingerprints were not dependent on DNA sorption, making them impractical for deducing the DNA-IR fingerprint. Finally, a DNA-IR fingerprint can be produced even from heterogeneous sedimentary materials. This can be used to monitor DNA on heterogeneous sorbents (minerals or organics) and detect DNA conformational changes, leaching potential, degradation, and protection against DNases (Schmidt and Martínez, 2017; Ye et al., 2011). Using this DNA-IR fingerprint, in combination with a real-time reaction vessel set up (e.g., Gillgren and Gorzsás, 2016), makes live monitoring of DNA sorption/desorption possible.

5. Recommendations

Based on the influence of minerals and organic contents on DNA sorption in lake sediments, the following is recommended before taxa identification.

1. Extract a potential clay mineral-rich subsample from the bulk sample. This is done by collecting fine particles (clay fraction), for

example, based on Stokes' law (detailed steps are included in Appendix A7).

2. Verify that the collected subsample is indeed rich in clay minerals (e.g., by XRD). The clay mineral-rich fraction might be present in relatively coarse particles due to clay-mineral or organo-clay complexes.
3. Although not addressed here, optimize DNA extraction protocols for clay mineral-rich samples.

6. Conclusion

The role of sediment geochemistry on DNA sorption was analyzed for bulk and size-fractionated samples. The sediments contained variable amounts of minerals and organic matter. In general, clay minerals were the preferential sedimentary components to bind DNA. Even more, DNA sorption onto the various size fractions was shown to be clay mineral-specific. In the Hotagen sediments, mica was the main DNA sorbent, regardless of size fraction, while chlorite had prominent DNA binding roles in size fractions greater than 16 μm . This is possibly due to the heterogeneity of lake sediments and the presence of clay-mineral and organo-clay mineral complexes. Furthermore, these complexes might affect the role of sedimentary OM in either increasing DNA sorption by expanding the surface area or in decreasing DNA sorption by covering

mineral surfaces. Additionally, IR peaks of the DNA amine bands in the 1640 and 1416 cm^{-1} regions evidenced DNA sorption. Significant shifts of these peaks were seen between the initial, control, and DNA treated samples by multivariate statistical analysis using MCR-ALS. The main DNA-IR peaks (1055 and 1231 cm^{-1}) were detected only after spectral subtraction. Indeed, the resulting DNA-IR fingerprint spectra were comparable to the salmon sperm DNA used in the sorption experiment. This distinct DNA-IR fingerprint can be produced even in heterogeneous sediments where the DNA-IR peaks overlap with mineral- and OM-IR peaks. Consequently, this fingerprint can be used to monitor DNA on sorbent surfaces. Additionally, a potential DNA-hotspot can be obtained in sedimentary materials based on mineral and organic contents. Using such hotspots for focusing sampling will increase the detection probability and precision, especially for rare taxa. Therefore, it is crucial to couple DNA findings in paleo-ecology studies (e.g., sedaDNA) to geochemical properties of sediments, mainly mineralogy.

Declaration of competing interest

The authors declare that they have no known competing financial interests or personal relationships that could have appeared to influence the work reported in this paper.

Acknowledgement

This research was funded by the Kempe Foundation (grant JCK-1821); the funding source had no involvement in the study design, writing of the report, and decision to submit the article for publication. The authors acknowledge Ms. Sarah Haddad from the Research and Analysis Platform for Environmental Sciences (PRASE, the Lebanese University, Lebanon) for grain size distribution analysis, Mr. Thai Tran Le for sediment size-separation experiments, Dr. András Gorzsás from the Vibrational Spectroscopy Core Facility (ViSP, Umeå University, Sweden) for valuable help with DRIFT spectra acquisition, Dr. Jonatan Klaminder from the Ecology and Environmental Sciences department (EMG) for early discussions on the project, Dr. Rolf Zale and Mr. Stefano Brignone (EMG) for providing the coring equipment and participating in sediment coring, and the editor and two anonymous reviewers for their critical review and constructive comments that improved the quality of this paper.

Appendix A. Supplementary data

Supplementary data to this article can be found online at <https://doi.org/10.1016/j.apgeochem.2020.104728>.

References

- Alsos, I.G., Lammers, Y., Yoccoz, N.G., Jørgensen, T., Sjögren, P., Gielly, L., Edwards, M. E., 2018. Plant DNA metabarcoding of lake sediments: how does it represent the contemporary vegetation. *PLoS One* 13, 1–23. <https://doi.org/10.1371/journal.pone.0195403>.
- Anderson, J.U., 1961. An improved pretreatment for mineralogical analysis of samples containing organic matter. *Clay Clay Miner.* 10, 380–388. <https://doi.org/10.1346/CCMN.1961.0100134>.
- Banyay, M., Sarkar, M., Gräslund, A., 2003. A library of IR bands of nucleic acids in solution. *Biophys. Chem.* 104, 477–488. [https://doi.org/10.1016/S0301-4622\(03\)00035-8](https://doi.org/10.1016/S0301-4622(03)00035-8).
- Benetoli, L.O. de B., De Santana, H., Zaia, C.T.B.V., Zaia, D.A.M., 2008. Adsorption of nucleic acid bases on clays: an investigation using Langmuir and Freundlich isotherms and FT-IR spectroscopy. *Monatsh. Chem.* 139, 753–761. <https://doi.org/10.1007/s00706-008-0862-z>.
- Bergaya, F., Lagaly, G., 2013. Purification of natural clays. In: Bergaya, F., Lagaly, G. (Eds.), *Handbook of Clay Science. Part A: Fundamentals*. Elsevier, pp. 213–242. <https://doi.org/10.1016/B978-0-08-098258-8.00008-0>.
- Boere, A.C., Rijpstra, W.I.C., De Lange, G.J., Sinnighe Damsté, J.S., Coolen, M.J.L., 2011. Preservation potential of ancient plankton DNA in Pleistocene marine sediments. *Geobiology* 9, 377–393. <https://doi.org/10.1111/j.1472-4669.2011.00290.x>.
- Cai, P., Huang, Q., Zhang, X., 2006a. Microcalorimetric studies of the effects of MgCl_2 concentrations and pH on the adsorption of DNA on montmorillonite, kaolinite and goethite. *Appl. Clay Sci.* 32, 147–152. <https://doi.org/10.1016/j.clay.2005.11.004>.
- Cai, P., Huang, Q., Zhang, X., Chen, H., 2006b. Adsorption of DNA on clay minerals and various colloidal particles from an Alfisol. *Soil Biol. Biochem.* 38, 471–476. <https://doi.org/10.1016/j.soilbio.2005.05.019>.
- Cai, P., Huang, Q.Y., Zhang, X.W., 2006c. Interactions of DNA with clay minerals and soil colloidal particles and protection against degradation by DNase. *Environ. Sci. Technol.* 40, 2971–2976. <https://doi.org/10.1021/es0522985>.
- Clarke, C.L., Edwards, M.E., Brown, A.G., Gielly, L., Lammers, Y., Heintzman, P.D., Ancin-Murguzur, F.J., Bråthen, K.A., Goslar, T., Alsos, I.G., 2019a. Holocene floristic diversity and richness in northeast Norway revealed by sedimentary ancient DNA (sedaDNA) and pollen. *Boreas* 48, 299–316. <https://doi.org/10.1111/bor.12357>.
- Clarke, C.L., Edwards, M.E., Gielly, L., Ehrlich, D., Hughes, P.D.M., Morozova, L.M., Hafliadason, H., Mangerud, J., Svendsen, J.I., Alsos, I.G., 2019b. Persistence of arctic-alpine flora during 24,000 years of environmental change in the Polar Urals. *Sci. Rep.* 9, 19613. <https://doi.org/10.1038/s41598-019-55989-9>.
- Combs, L.G., Warren, J.E., Huynh, V., Castaneda, J., Golden, T.D., Roby, R.K., 2015. The effects of metal ion PCR inhibitors on results obtained with the Quantifiler® Human DNA Quantification Kit. *Forensic Sci. Int. Genet.* 19, 180–189. <https://doi.org/10.1016/j.fsigen.2015.06.013>.
- Crecchio, C., Ruggiero, P., Curci, M., Colombo, C., Palumbo, G., Stotzky, G., 2005. Binding of DNA from montmorillonite–humic acids–Aluminum or Iron hydroxypolymers. *Soil Sci. Soc. Am. J.* 69, 834. <https://doi.org/10.2136/sssaj2004.0166>.
- Deiner, K., Bik, H.M., Mächler, E., Seymour, M., Lacoursière-Roussel, A., Altermatt, F., Creer, S., Bista, I., Lodge, D.M., de Vere, N., Pfrender, M.E., Bernatchez, L., 2017. Environmental DNA metabarcoding: Transforming how we survey animal and plant communities. *Mol. Ecol.* 26, 5872–5895. <https://doi.org/10.1111/mec.14350>.
- Doebelin, N., Kleeberg, R., 2015. Profex: a graphical user interface for the Rietveld refinement program BGMN. *J. Appl. Crystallogr.* 48, 1573–1580. <https://doi.org/10.1107/S1600576715014685>.
- Drever, J.I., Vance, G.F., 1994. Role of soil organic acids in mineral weathering processes. In: Pittman, E.D., Lewan, M.D. (Eds.), *Organic Acids in Geological Processes*. Springer Berlin Heidelberg, Berlin, Heidelberg, pp. 138–161. https://doi.org/10.1007/978-3-642-78356-2_6.
- Felten, J., Hall, H., Jaumot, J., Tauler, R., de Juan, A., Gorzsás, A., 2019. Addendum: Vibrational spectroscopic image analysis of biological material using multivariate curve resolution–alternating least squares (MCR-ALS). *Nat. Protoc.* 14, 3032. <https://doi.org/10.1038/s41596-019-0196-9>.
- Felten, J., Hall, H., Jaumot, J., Tauler, R., De Juan, A., Gorzsás, A., 2015. Vibrational spectroscopic image analysis of biological material using multivariate curve resolution–alternating least squares (MCR-ALS). *Nat. Protoc.* 10, 217–240. <https://doi.org/10.1038/nprot.2015.008>.
- Franchi, M., Bramanti, E., Bonzi, L.M., Orioli, P.L., Vettori, C., Gallori, E., 1999. Clay-nucleic acid complexes: characteristics and implications for the preservation of genetic material in primeval habitats. *Orig. Life Evol. Biosph.* 29, 297–315. <https://doi.org/10.1023/A:1006557832574>.
- Freeman, Dieudonné, Collins, Sand, K., 2020. Survival of environmental DNA in natural environments: surface charge and topography of minerals as driver for DNA storage. *bioRxiv* 18. <https://doi.org/10.1101/2020.01.28.922997>.
- Giguet-Covex, C., Ficetola, G.F., Walsh, K., Poulenard, J., Bajard, M., Fouinat, L., Sabatier, P., Gielly, L., Messenger, E., Develle, A.L., David, F., Taberlet, P., Brisset, E., Guiter, F., Sinet, R., Arnaud, F., 2019. New insights on lake sediment DNA from the catchment: importance of taphonomic and analytical issues on the record quality. *Sci. Rep.* 9, 14676. <https://doi.org/10.1038/s41598-019-50339-1>.
- Giguet-Covex, C., Pansu, J., Arnaud, F., Rey, P.-J., Griggo, C., Gielly, L., Domaizon, I., Coissac, E., David, F., Choler, P., Poulenard, J., Taberlet, P., 2014. Long livestock farming history and human landscape shaping revealed by lake sediment DNA. *Nat. Commun.* 5, 3211. <https://doi.org/10.1038/ncomms4211>.
- Gillgren, T., Gorzsás, A., 2016. A one-pot set-up for real-time reaction monitoring by FTIR spectroscopy. *Wood Sci. Technol.* 50, 567–580. <https://doi.org/10.1007/s00226-016-0801-9>.
- Han, Y., Han, L., Yao, Y., Li, Y., Liu, X., 2018. Key factors in FTIR spectroscopic analysis of DNA: the sampling technique, pretreatment temperature and sample concentration. *Anal. Methods* 10, 2436–2443. <https://doi.org/10.1039/C8AY00386F>.
- Huang, Y.T., Lowe, D.J., Churchman, G.J., Schipper, L.A., Cursons, R., Zhang, H., Chen, T.Y., Cooper, A., 2016. DNA adsorption by nanocrystalline allophane spherules and nanoaggregates, and implications for carbon sequestration in Andisols. *Appl. Clay Sci.* 120, 40–50. <https://doi.org/10.1016/j.clay.2015.11.009>.
- Huerlimann, R., Cooper, M.K., Edmunds, R.C., Villacorta-Rath, C., Le Port, A., Robson, H. L.A., Strugnell, J.M., Burrows, D., Jerry, D.R., 2020. Enhancing tropical conservation and ecology research with aquatic environmental DNA methods: an introduction for non-environmental DNA specialists. *Anim. Conserv.* <https://doi.org/10.1111/acv.12583>.
- Kisand, V., Talas, L., Kisand, A., Stivrins, N., Reitalu, T., Alliksaar, T., Vassiljev, J., Liiv, M., Heinsalu, A., Seppä, H., Veski, S., 2018. From microbial eukaryotes to metazoan vertebrates: Wide spectrum paleo-diversity in sedimentary ancient DNA over the last ~14,500 years. *Geobiology* 16, 628–639. <https://doi.org/10.1111/gbi.12307>.
- Levy-Booth, D.J., Campbell, R.G., Gulden, R.H., Hart, M.M., Powell, J.R., Klironomos, J. N., Pauls, K.P., Swanton, C.J., Trevors, J.T., Dunfield, K.E., 2007. Cycling of extracellular DNA in the soil environment. *Soil Biol. Biochem.* 39, 2977–2991. <https://doi.org/10.1016/j.soilbio.2007.06.020>.

- Margenot, A.J., Parikh, S.J., Calderón, F.J., 2019. Improving infrared spectroscopy characterization of soil organic matter with spectral subtractions. *JoVE*. <https://doi.org/10.3791/57464>.
- Mikutta, R., Kleber, M., Kaiser, K., Jahn, R., 2005. Review: organic matter removal from soils using hydrogen peroxide, sodium hypochlorite, and disodium peroxodisulfate. *Soil Sci. Soc. Am. J.* 69, 120. <https://doi.org/10.2136/sssaj2005.0120>.
- Olajos, F., Bokma, F., Bartels, P., Myrstener, E., Rydberg, J., Öhlund, G., Bindler, R., Wang, X.-R., Zale, R., Englund, G., 2018. Estimating species colonization dates using DNA in lake sediment. *Methods Ecol. Evol.* 9, 535–543. <https://doi.org/10.1111/2041-210X.12890>.
- Pansu, M., Gautheyrou, J., 2006. Mineralogical characterisations by X-Ray diffractometry. In: *Handbook of Soil Analysis*. Springer Berlin Heidelberg, Berlin, Heidelberg, pp. 83–131. https://doi.org/10.1007/978-3-540-31211-6_4.
- Parducci, L., Alsos, I.G., Unneberg, P., Pedersen, M.W., Han, L., Lammers, Y., Salonen, J. S., Väiliranta, M.M., Slotte, T., Wohlfarth, B., 2019. Shotgun environmental DNA, pollen, and macrofossil analysis of lateglacial lake sediments from southern Sweden. *Front. Ecol. Evol.* 7 <https://doi.org/10.3389/fevo.2019.00189>.
- Parducci, L., Bennett, K.D., Ficetola, G.F., Alsos, I.G., Suyama, Y., Wood, J.R., Pedersen, M.W., 2017. Ancient plant DNA in lake sediments. *New Phytol.* 214, 924–942. <https://doi.org/10.1111/nph.14470>.
- Parducci, L., Nota, K., Wood, J., 2018. Reconstructing past vegetation communities using ancient DNA from lake sediments. https://doi.org/10.1007/13836_2018_38.
- Pedersen, M.W., Ginolhac, A., Orlando, L., Olsen, J., Andersen, K., Holm, J., Funder, S., Willerslev, E., Kjær, K.H., 2013. A comparative study of ancient environmental DNA to pollen and macrofossils from lake sediments reveals taxonomic overlap and additional plant taxa. *Quat. Sci. Rev.* 75, 161–168. <https://doi.org/10.1016/j.quascirev.2013.06.006>.
- Pedreira-Segade, U., Hao, J., Razafitianamaharavo, A., Pelletier, M., Marry, V., Le-Crom, S., Michot, L.J., Daniel, I., 2018. How do nucleotides adsorb onto clays? *Life* 8, 59. <https://doi.org/10.3390/life8040059>.
- Pietramellara, G., Ascher, J., Borgogni, F., Ceccherini, M.T., Guerri, G., Nannipieri, P., 2009. Extracellular DNA in soil and sediment: fate and ecological relevance. *Biol. Fertil. Soils* 45, 219–235. <https://doi.org/10.1007/s00374-008-0345-8>.
- Post, J.E., Bish, D.L., 1989. Rietveld refinement of crystal structures using powder X-ray diffraction data. *Mod. Powder Diffr.* 20, 277–308.
- Rosén, P., Vogel, H., Cunningham, L., Reuss, N., Conley, D.J., Persson, P., 2010. Fourier transform infrared spectroscopy, a new method for rapid determination of total organic and inorganic carbon and biogenic silica concentration in lake sediments. *J. Paleolimnol.* 43, 247–259. <https://doi.org/10.1007/s10933-009-9329-4>.
- Saeki, K., Kunito, T., Sakai, M., 2011. Effect of tris-HCl buffer on DNA adsorption by a variety of soil constituents. *Microb. Environ.* 26, 88–91. <https://doi.org/10.1264/j sme2.ME10172>.
- Saeki, K., Sakai, M., Wada, S.I., 2010. DNA adsorption on synthetic and natural allophanes. *Appl. Clay Sci.* 50, 493–497. <https://doi.org/10.1016/j.clay.2010.09.015>.
- Schmidt, M.P., Martínez, C.E., 2017. Ironing out genes in the environment: an experimental study of the DNA-goethite interface. *Langmuir* 33, 8525–8532. <https://doi.org/10.1021/acs.langmuir.7b01911>.
- Sheng, X., Qin, C., Yang, B., Hu, X., Liu, C., Waigi, M.G., Li, X., Ling, W., 2019. Metal cation saturation on montmorillonites facilitates the adsorption of DNA via cation bridging. *Chemosphere* 235, 670–678. <https://doi.org/10.1016/j.chemosphere.2019.06.159>.
- Slon, V., Hopfé, C., Weiß, C.L., Mafessoni, F., De La Rasilla, M., Lalueza-Fox, C., Rosas, A., Soressi, M., Knul, M.V., Miller, R., Stewart, J.R., Derevianko, A.P., Jacobs, Z., Li, B., Roberts, R.G., Shunkov, M.V., De Lumley, H., Perrenoud, C., Gusić, I., Kučan, Z., Rudan, P., Aximu-Petri, A., Essel, E., Nagel, S., Nickel, B., Schmidt, A., Prüfer, K., Kelso, J., Burbano, H.A., Pääbo, S., Meyer, M., 2017. Neandertal and denisovan DNA from Pleistocene sediments. *Science* 356, 605–608. <https://doi.org/10.1126/science.aam9695>.
- Torti, A., Lever, M.A., Jørgensen, B.B., 2015. Origin, dynamics, and implications of extracellular DNA pools in marine sediments. *Mar. Genomics* 24, 185–196. <https://doi.org/10.1016/j.margen.2015.08.007>.
- Vogel, H., Rosén, P., Wagner, B., Melles, M., Persson, P., 2008. Fourier transform infrared spectroscopy, a new cost-effective tool for quantitative analysis of biogeochemical properties in long sediment records. *J. Paleolimnol.* 40, 689–702. <https://doi.org/10.1007/s10933-008-9193-7>.
- Voldstad, L.H., Alsos, I.G., Farnsworth, W.R., Heintzman, P.D., Håkansson, L., Kjellman, S.E., Rouillard, A., Schomacker, A., Eidesen, P.B., 2020. A complete Holocene lake sediment ancient DNA record reveals long-standing high Arctic plant diversity hotspot in northern Svalbard. *Quat. Sci. Rev.* 234, 106207. <https://doi.org/10.1016/j.quascirev.2020.106207>.
- Xie, H., Wan, Z., Liu, S., Zhang, Y., Tan, J., Yang, H., 2019. Charge-dependent regulation in DNA adsorption on 2D clay minerals. *Sci. Rep.* 9, 1–10. <https://doi.org/10.1038/s41598-019-41093-5>.
- Xu, H., 2010. Synergistic roles of microorganisms in mineral precipitates associated with deep sea methane seeps. In: *Geomicrobiology: Molecular and Environmental Perspective*. Springer Netherlands, Dordrecht, pp. 325–346. https://doi.org/10.1007/978-90-481-9204-5_15.
- Xue, J., Feng, Y., 2018. Determination of adsorption and desorption of DNA molecules on freshwater and marine sediments. *J. Appl. Microbiol.* 124, 1480–1492. <https://doi.org/10.1111/jam.13739>.
- Ye, M., Li, B., Zhang, Y., Li, H., Wang, X., Hu, J., 2011. Confined water nanofilm promoting nonenzymatic degradation of DNA molecules. *J. Phys. Chem. B* 115, 2754–2758. <https://doi.org/10.1021/jp109212d>.
- Yu, W.H., Li, N., Tong, D.S., Zhou, C.H., Lin, C.X., Xu, C.Y., 2013. Adsorption of proteins and nucleic acids on clay minerals and their interactions: a review. *Appl. Clay Sci.* 80–81, 443–452. <https://doi.org/10.1016/j.clay.2013.06.003>.

Appendix A. Supplementary Data

Geochemical identification of potential DNA-hotspots and DNA-infrared fingerprints in lake sediments

Hussein Jaafar Kanbar^{a,*}, Fredrik Olajos^b, Göran Englund^b, Michael Holmboe^{a,*}

a. Department of Chemistry, Umeå University, SE-901 87, Umeå, Sweden

b. Department of Ecology & Environmental Sciences, Umeå University, Umeå, Sweden;
goran.englund@umu.se, fredrik.olajos@umu.se.

*Correspondence: hussein.kanbar@umu.se, michael.holmboe@umu.se

DOI: [10.1016/j.apgeochem.2020.104728](https://doi.org/10.1016/j.apgeochem.2020.104728)

ORCID

Hussein J. Kanbar: orcid.org/0000-0002-9505-9974

Fredrik Olajos: orcid.org/0000-0003-2001-5077

Göran Englund: orcid.org/0000-0001-5634-8602

Michael Holmboe: orcid.org/0000-0003-3927-6197

Content

A1: Sedimentary organic matter removal by sodium hypochlorite (NaOCl)	1
A2: Salmon sperm DNA sorption onto sediments.....	2
A3: Infrared spectral subtraction to determine the DNA-IR fingerprint	3
A4: Regression analysis data for clay minerals and DNA sorption (DNA _s and DNA _{s-inorg})	4
A5: Correlation coefficients for the PCA plots.....	5
A6: Multiple linear regression statistics for theoretical and experimental DNA sorption values	9
A7: Detailed steps for the collection of selected particle sizes.....	11
Fig. A.1: Variation of DNA _s , DNA _{s-inorg} , ΣClays (chlorite+mica), ΣQuartz and feldspars, and organic matter (OM) for different size fractions as a function of sediment depth.....	13
Fig. A.2: Diffuse reflectance infrared Fourier transform (DRIFT) spectra for the initial compounds used in the DNA sorption experiment	14
References.....	15

A1: Sedimentary organic matter removal by sodium hypochlorite (NaOCl)

Sedimentary organic matter was removed from the bulk and size-fractionated sediments. The initial sediments are named Sed and the ones after organic matter (OM) removal are named Sed_{inorg}. Several methods are found in the literature to remove OM from soils and sediments (e.g., Mikutta et al., 2005). In our case, we are aiming for a method that will result in minimal mineral alteration. Therefore, we used a relatively gentle method, which is NaOCl treatment. Even though chemical treatment by NaOCl does not remove all the organic matter, it does not cause a change in the mineral structure of the matrix, like ashing (thermal combustion) or H₂O₂ treatment would do (Margenot et al., 2015; Mikutta et al., 2005). The steps for OM removal via NaOCl is included in Margenot et al. (2019).

A2: Salmon sperm DNA sorption onto sediments

The low molecular weight salmon sperm DNA solution (200 µg/ml, ~2000 base pair; CAS 100403-24-5; Sigma Aldrich) was prepared in 10 mM Tris base buffer (trisaminomethane) and 25 mM CaCl₂. The pH was adjusted to 8 by 1 M HCl. In 2 ml Eppendorf tubes, 2 ml of the solution was added to 8 mg of sediments (for i. initial sediments named Sed and for ii. sediments after organic matter removal named Sed_{inorg}) and mixed in an end-over-end shaker for 2 hours (under dark conditions, 25°C). The Eppendorf tubes were then centrifuged at 20,000 g for 25 minutes. The supernatants were used to determine the remaining DNA concentrations. The final DNA concentrations (DNA_f) were quantified by absorbance at 260 nm (A₂₆₀) using a UV spectrophotometer (Lambda 750 UV/Vis/NIR spectrometer by Perkin Elmer); standards of known DNA concentrations were prepared from the stock solution. The turbidity (at A₃₂₀) was subtracted from A₂₆₀ before calculating the DNA concentration. The experimental conditions are based on other studies (Cai et al., 2006; Pedreira-Segade et al., 2018); the same references also include information on the quantification of DNA in solution. The purity of DNA in the solutions was verified by A₂₆₀/A₂₈₀ ratios higher than 1.8. The sorbed DNA contents on Sed and Sed_{inorg} were calculated per dry sediment mass using the following equation

$$DNA_s = (DNA_i - DNA_f) \times \frac{V}{m}$$

Where DNA_s is the sorbed DNA content (µg/mg), DNA_i and DNA_f are the initial and final concentrations of DNA (µg/ml), respectively, V is the volume of the solution used in the sorption experiment (ml), and m is the mass of the sediment used (mg). The sorbed DNA contents onto Sed and Sed_{inorg} are named DNA_s and DNA_{s-inorg}, respectively.

A3: Infrared spectral subtraction to determine the DNA-IR fingerprint

The DNA infrared (IR) fingerprints of the sediments were produced by spectral subtraction of the control samples (-Ctr) from the DNA treated samples (-DNA). Here, we highlight the importance of control treatment; the control treatment included sediments mixed with solutions containing 10 mM Tris and 25 mM CaCl₂, but did not contain any DNA. The experimental conditions, i.e., shaking time, centrifugation, and freeze-drying, were similar to the DNA treated samples. That way, the obtained DNA-IR fingerprint solely belongs to the IR change caused by DNA sorption and is not influenced by Tris nor by CaCl₂. Spectral subtraction was done on Opus 7.0 after normalization using the MCR-ALS GUI provided by the Vibration Spectroscopy Core Facility at Umeå University (www.umu.se/en/research/infrastructure/visp/downloads/). The spectra were normalized according to the regional maximum represented by the Si-O stretching peak at the 1150-950 cm⁻¹ region. Although several researchers discuss modifying the subtraction factor (SF) to zero-out, cancel, or reduce mineral peak interferences (e.g., Margenot et al., 2019, 2016; Padilla et al., 2014; Smith, 1998), this was not necessary in our case because normalization was done using the MCR-ALS GUI. Therefore, SF was = 1 in all cases. Indeed, the mineral interference of quartz (2000-1780 cm⁻¹ and 800 cm⁻¹) was zeroed-out in the subtracted spectra, as suggested, for example, by Margenot et al. (2016) and Nguyen et al. (1991). Another note is that each subtracted spectrum was produced from the same sample (i.e., same depth and same size-fraction), thus, there was no change in mineral or organic composition. Therefore, the product spectra represent the change solely caused by DNA sorption.

A4: Regression analysis data for clay minerals and DNA sorption (DNA_s and DNA_{s-inorg})

This section includes the statistical data for the correlation between DNA sorption (DNA_s and DNA_{s-inorg}) and ΣClays that are presented in Fig. 5a in the main text.

DNA_s: DNA sorbed onto sediments (Sed).

DNA_{s-inorg}: DNA sorbed onto sediments after the removal of organic matter (Sed_{inorg}).

ΣClays: the sum of mica and chlorite (quantified by XRD-Profex).

1. DNA_s and ΣClays

Regression statistics							
Multiple R	0.815						
R Square	0.664						
Adjusted R Square	0.658						
Standard Error	2.979						
Observations	60						

ANOVA					
	<i>df</i>	<i>SS</i>	<i>MS</i>	<i>F</i>	<i>Significance F</i>
Regression	1	1017.02	1017.02	114.59	2.34E-15
Residual	58	514.76	8.88		
Total	59	1531.78			

	<i>Coefficients</i>	<i>Standard Error</i>	<i>t Stat</i>	<i>P-value</i>	<i>Lower 95%</i>	<i>Upper 95%</i>	<i>Lower 95.0%</i>	<i>Upper 95.0%</i>
Intercept	3.13	1.16	2.70	9.17E-03	0.81	5.45	0.81	5.45
ΣClays	0.26	0.02	10.70	2.34E-15	0.21	0.31	0.21	0.31

2. DNA_{s-inorg} and ΣClays

Regression statistics							
Multiple R	0.858						
R Square	0.737						
Adjusted R Square	0.732						
Standard Error	2.184						
Observations	60						

ANOVA					
	<i>df</i>	<i>SS</i>	<i>MS</i>	<i>F</i>	<i>Significance F</i>
Regression	1	774.04	774.04	162.23	1.90E-18
Residual	58	276.74	4.77		
Total	59	1050.78			

	<i>Coefficients</i>	<i>Standard Error</i>	<i>t Stat</i>	<i>P-value</i>	<i>Lower 95%</i>	<i>Upper 95%</i>	<i>Lower 95.0%</i>	<i>Upper 95.0%</i>
Intercept	3.51	0.85	4.12	1.20E-04	1.80	5.21	1.80	5.21
ΣClays	0.23	0.02	12.74	1.90E-18	0.19	0.27	0.19	0.27

A5: Correlation coefficients for the PCA plots

This part includes 1) the principal component analysis (PCA) correlation coefficients for chlorite, mica, albite, quartz, K-feldspars, the sum of clay minerals (Σ Clays = chlorite + mica), organic matter (OM), and DNA sorption (DNA_s), 2) the percentage of variance for the PCA plots (Fig. 5b in the main text), and 3) the non-parametric Spearman correlation. Each table represents the correlation coefficients for one size fraction (n=12 for each size fraction). Albite and K-Feldspars are both feldspar minerals; in the text and in the tables below, only the sum of feldspars is used (i.e., feldspars = albite + K-feldspars).

1. PCA correlation matrix

0-4 μm	Mica	Albite	Quartz	K-Feldspars	ΣClays	OM	DNA_s
Chlorite	-0.584	0.213	-0.381	0.429	-0.288	-0.098	-0.141
Mica		-0.859	0.042	-0.942	0.946	0.638	0.687
Albite			-0.098	0.860	-0.928	-0.884	-0.851
Quartz				-0.054	-0.103	0.238	0.134
K-Feldspars					-0.939	-0.597	-0.663
ΣClays						0.713	0.754
OM							0.902

4-16 μm	Mica	Albite	Quartz	K-Feldspars	ΣClays	OM	DNA_s
Chlorite	-0.564	0.404	-0.059	0.129	-0.300	-0.533	-0.577
Mica		-0.974	-0.588	-0.833	0.957	0.790	0.870
Albite			0.606	0.888	-0.983	-0.781	-0.838
Quartz				0.606	-0.700	-0.487	-0.619
K-Feldspars					-0.916	-0.657	-0.691
ΣClays						0.725	0.803
OM							0.965

16-64 μm	Mica	Albite	Quartz	K-Feldspars	ΣClays	OM	DNA_s
Chlorite	0.233	-0.681	-0.003	-0.292	0.581	0.509	0.667
Mica		-0.683	-0.592	-0.544	0.927	0.525	0.799
Albite			0.143	0.239	-0.835	-0.614	-0.847
Quartz				0.069	-0.496	-0.144	-0.391
K-Feldspars					-0.568	-0.545	-0.548
ΣClays						0.636	0.926
OM							0.832

>64 μm	Mica	Albite	Quartz	K-Feldspars	ΣClays	OM	DNA_s
Chlorite	0.795	-0.299	-0.796	-0.675	0.910	0.683	0.919
Mica		-0.510	-0.702	-0.713	0.975	0.681	0.856
Albite			-0.001	0.149	-0.458	-0.190	-0.314
Quartz				0.349	-0.772	-0.624	-0.885
K-Feldspars					-0.735	-0.541	-0.571
ΣClays						0.716	0.922
OM							0.795

2. Percentage of variance for the PCA data

	% of variance			
	0-4 μm	4-16 μm	16-64 μm	>64 μm
PC 1	65.05	73.58	62.03	70.42
PC 2	16.65	15.43	15.99	13.42

3. Spearman correlation

0-4 μm		Mica	Albite	Quartz	K-Feldspars	ΣClays	OM	DNA_s
Chlorite	Rho (ρ)	-.587*	0.189	-0.105	0.287	-0.098	-0.025	-0.014
	<i>P</i>	0.045	0.557	0.746	0.366	0.762	0.940	0.966
Mica	Rho (ρ)		-.741**	-0.175	-.804**	.818**	0.515	.622*
	<i>P</i>		0.006	0.587	0.002	0.001	0.087	0.031
Albite	Rho (ρ)			-0.168	.783**	-.853**	-.722**	-.804**
	<i>P</i>			0.602	0.003	0.000	0.008	0.002
Quartz	Rho (ρ)				0.077	-0.105	0.326	0.077
	<i>P</i>				0.812	0.746	0.301	0.812
K-Feldspars	Rho (ρ)					-.895**	-.613*	-.608*
	<i>P</i>					0.000	0.034	0.036
ΣClays	Rho (ρ)						.715**	.846**
	<i>P</i>						0.009	0.001
OM	Rho (ρ)							.746**
	<i>P</i>							0.005

Rho (ρ): Spearman's rho.

P: P value. The P value is the probability of finding the observed results when the null hypothesis (H₀) is true.

H₀: there does not exist a correlation between X and Y.

** : Correlation is significant at the 0.01 level (2-tailed).

* : Correlation is significant at the 0.05 level (2-tailed).

4-16 μm		Mica	Albite	Quartz	K-Feldspars	ΣClays	OM	DNA_s
Chlorite	Rho (ρ)	-.620*	0.462	-0.200	0.116	-0.238	0.032	-0.221
	<i>P</i>	0.032	0.130	0.534	0.721	0.456	0.923	0.491
Mica	Rho (ρ)		-.951**	-0.497	-.727**	.895**	.601*	.776**
	<i>P</i>		0.000	0.101	0.007	0.000	0.039	0.003
Albite	Rho (ρ)			0.538	.734**	-.944**	-.706*	-.755**
	<i>P</i>			0.071	0.007	0.000	0.010	0.005
Quartz	Rho (ρ)				0.538	-.636*	-.797**	-.839**
	<i>P</i>				0.071	0.026	0.002	0.001
K-Feldspars	Rho (ρ)					-.811**	-.643*	-.580*
	<i>P</i>					0.001	0.024	0.048
ΣClays	Rho (ρ)						.713**	.769**
	<i>P</i>						0.009	0.003
OM	Rho (ρ)							.853**
	<i>P</i>							0.000

16-64 μm		Mica	Albite	Quartz	K-Feldspars	ΣClays	OM	DNA_s
Chlorite	Rho (ρ)	0.517	-.755**	-0.014	-0.301	.720**	0.503	.671*
	<i>P</i>	0.085	0.005	0.966	0.342	0.008	0.095	0.017
Mica	Rho (ρ)		-.867**	-0.476	-0.552	.902**	0.294	.860**
	<i>P</i>		0.000	0.118	0.063	0.000	0.354	0.000
Albite	Rho (ρ)			0.350	0.364	-.951**	-0.455	-.937**
	<i>P</i>			0.265	0.245	0.000	0.138	0.000
Quartz	Rho (ρ)				-0.084	-0.455	0.315	-0.448
	<i>P</i>				0.795	0.138	0.319	0.145
K-Feldspars	Rho (ρ)					-0.524	-0.399	-0.448
	<i>P</i>					0.080	0.199	0.145
ΣClays	Rho (ρ)						0.427	.972**
	<i>P</i>						0.167	0.000
OM	Rho (ρ)							0.517
	<i>P</i>							0.085

>64 μm		Mica	Albite	Quartz	K-Feldspars	ΣClays	OM	DNA_s
Chlorite	Rho (ρ)	.755**	-0.210	-.762**	-.650*	.846**	.741**	.916**
	<i>P</i>	0.005	0.513	0.004	0.022	0.001	0.006	0.000
Mica	Rho (ρ)		-0.399	-.776**	-.671*	.965**	.685*	.790**
	<i>P</i>		0.199	0.003	0.017	0.000	0.014	0.002
Albite	Rho (ρ)			-0.028	0.133	-0.413	-0.462	-0.231
	<i>P</i>			0.931	0.681	0.183	0.131	0.471
Quartz	Rho (ρ)				0.336	-.839**	-.629*	-.874**
	<i>P</i>				0.286	0.001	0.028	0.000
K-Feldspars	Rho (ρ)					-.615*	-0.371	-0.462
	<i>P</i>					0.033	0.236	0.131
ΣClays	Rho (ρ)						.769**	.881**
	<i>P</i>						0.003	0.000
OM	Rho (ρ)							.762**
	<i>P</i>							0.004

A6: Multiple linear regression statistics for theoretical and experimental DNA sorption values

Below are the statistical data for the multiple linear regressions of the theoretical and experimental DNA sorption values (Fig. 6 in the main text).

1. Explanatory variables: chlorite and mica (Fig. 6a)

Regression statistics	
Multiple R	0.816
R Square	0.666
Adjusted R Square	0.654
Standard Error	2.995
Observations	60

ANOVA					
	<i>df</i>	<i>SS</i>	<i>MS</i>	<i>F</i>	<i>Significance F</i>
Regression	2	1020.46	510.23	56.88	2.63E-14
Residual	57	511.32	8.97		
Total	59	1531.78			

	<i>Coefficients</i>	<i>Standard Error</i>	<i>t Stat</i>	<i>P-value</i>	<i>Lower 95%</i>	<i>Upper 95%</i>	<i>Lower 95.0%</i>	<i>Upper 95.0%</i>
Intercept	3.31	1.20	2.75	7.94E-03	0.90	5.72	0.90	5.72
Chlorite	0.20	0.10	2.05	4.53E-02	0.00	0.40	0.00	0.40
Mica	0.28	0.04	7.31	9.61E-10	0.20	0.36	0.20	0.36

2. Explanatory variables: chlorite, mica, quartz, albite, and K-feldspars (Fig. 6b)

Regression statistics	
Multiple R	0.834
R Square	0.695
Adjusted R Square	0.667
Standard Error	2.942
Observations	60

ANOVA					
	<i>df</i>	<i>SS</i>	<i>MS</i>	<i>F</i>	<i>Significance F</i>
Regression	5	1064.29	212.86	24.59	8.12E-13
Residual	54	467.49	8.66		
Total	59	1531.78			

	<i>Coefficients</i>	<i>Standard Error</i>	<i>t Stat</i>	<i>P-value</i>	<i>Lower 95%</i>	<i>Upper 95%</i>	<i>Lower 95.0%</i>	<i>Upper 95.0%</i>
Intercept	-11.00	18.63	-0.59	5.57E-01	-48.35	26.34	-48.35	26.34
Chlorite	0.43	0.20	2.13	3.78E-02	0.03	0.83	0.03	0.83
Mica	0.41	0.19	2.11	3.92E-02	0.02	0.79	0.02	0.79
Quartz	0.27	0.21	1.32	1.92E-01	-0.14	0.69	-0.14	0.69
Albite	0.13	0.26	0.53	6.02E-01	-0.38	0.65	-0.38	0.65
K-feldspars	-0.10	0.31	-0.31	7.57E-01	-0.71	0.52	-0.71	0.52

3. Explanatory variables: chlorite, mica, and organic matter (Fig. 6c)

Regression statistics	
Multiple R	0.953
R Square	0.909
Adjusted R Square	0.904
Standard Error	1.581
Observations	60

ANOVA					
	<i>df</i>	<i>SS</i>	<i>MS</i>	<i>F</i>	<i>Significance F</i>
Regression	3	1391.82	463.94	185.62	4.62E-29
Residual	56	139.96	2.50		
Total	59	1531.78			

	<i>Coefficients</i>	<i>Standard Error</i>	<i>t Stat</i>	<i>P-value</i>	<i>Lower 95%</i>	<i>Upper 95%</i>	<i>Lower 95.0%</i>	<i>Upper 95.0%</i>
Intercept	-2.42	0.79	-3.07	3.32E-03	-4.01	-0.84	-4.01	-0.84
OM%	0.41	0.03	12.19	2.18E-17	0.34	0.48	0.34	0.48
Chlorite	0.23	0.05	4.42	4.54E-05	0.13	0.34	0.13	0.34
Mica	0.15	0.02	6.73	9.77E-09	0.11	0.20	0.11	0.20

4. Explanatory variables: chlorite, mica, quartz, albite, K-feldspar, and organic matter (Fig. 6d)

Regression statistics	
Multiple R	0.961
R Square	0.923
Adjusted R Square	0.914
Standard Error	1.493
Observations	60

ANOVA					
	<i>df</i>	<i>SS</i>	<i>MS</i>	<i>F</i>	<i>Significance F</i>
Regression	6	1413.66	235.61	105.71	1.08E-27
Residual	53	118.12	2.23		
Total	59	1531.78			

	<i>Coefficients</i>	<i>Standard Error</i>	<i>t Stat</i>	<i>P-value</i>	<i>Lower 95%</i>	<i>Upper 95%</i>	<i>Lower 95.0%</i>	<i>Upper 95.0%</i>
Intercept	-16.98	9.46	-1.79	7.85E-02	-35.96	2.00	-35.96	2.00
OM%	0.40	0.03	12.52	1.85E-17	0.34	0.47	0.34	0.47
Chlorite	0.43	0.10	4.17	1.14E-04	0.22	0.63	0.22	0.63
Mica	0.29	0.10	3.00	4.10E-03	0.10	0.49	0.10	0.49
Quartz	0.22	0.11	2.12	3.88E-02	0.01	0.43	0.01	0.43
Albite	0.17	0.13	1.34	1.86E-01	-0.09	0.44	-0.09	0.44
K-feldspars	-0.01	0.16	-0.09	9.29E-01	-0.33	0.30	-0.33	0.30

A7: Detailed steps for the collection of selected particle sizes

The particle size separation is based on Stokes' law (see Lagaly and Dékány (2013) p 258-261 for more information). The following formula is used,

$$t = \frac{18 \cdot \eta \cdot h}{(\rho_s - \rho_l)d^2g}$$

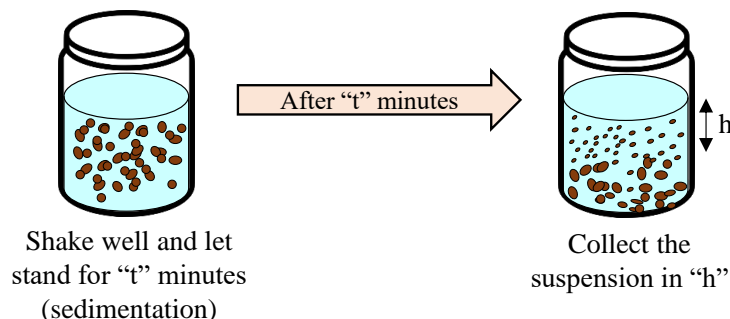
where: t is the time (in seconds) needed for particles to settle within the given distance h (in m, see figure below), η is the viscosity of the solution (in $\text{kg}\cdot\text{s}/\text{m}^2$), ρ_s and ρ_l are the particle and liquid densities (in kg/m^3), respectively, d is the particle cut-off size (in m), and g is the gravitational acceleration ($9.81 \text{ m}/\text{s}^2$).

In case the experiment is done at 25°C and water is used, then η and ρ_l can be taken as $0.00089 \text{ kg}\cdot\text{s}/\text{m}^2$ and $1000 \text{ kg}/\text{m}^3$, respectively. The value of ρ_s depends on the composition of the matrix. However, $2650 \text{ kg}/\text{m}^3$ ($2.65 \text{ g}/\text{cm}^3$) can be used for most soils and sediments (for example, the densities of quartz, feldspars, kaolinite, illite, chlorite, calcite, aragonite, and dolomite are 2.65, 2.56, 2.65, 2.75, 2.95, 2.71, 2.93, and $2.84 \text{ g}/\text{cm}^3$, respectively). It should be noted that organic matter rich samples have lower densities.

To avoid any contamination with airborne DNA, the steps included below must be done in sterile environments.

1. Add sterile Milli-Q water to $\sim 1 \text{ g}$ of fresh sample (sediment or soil) in a closed cylindrical container (e.g., glass bottle) and shake overnight.
2. Let the container stand for a specific period (sedimentation time, t) before collecting the suspension containing the desired particle sizes (in the sedimentation distance, h).

Time depends on the size of the particles to be collected as well as h .



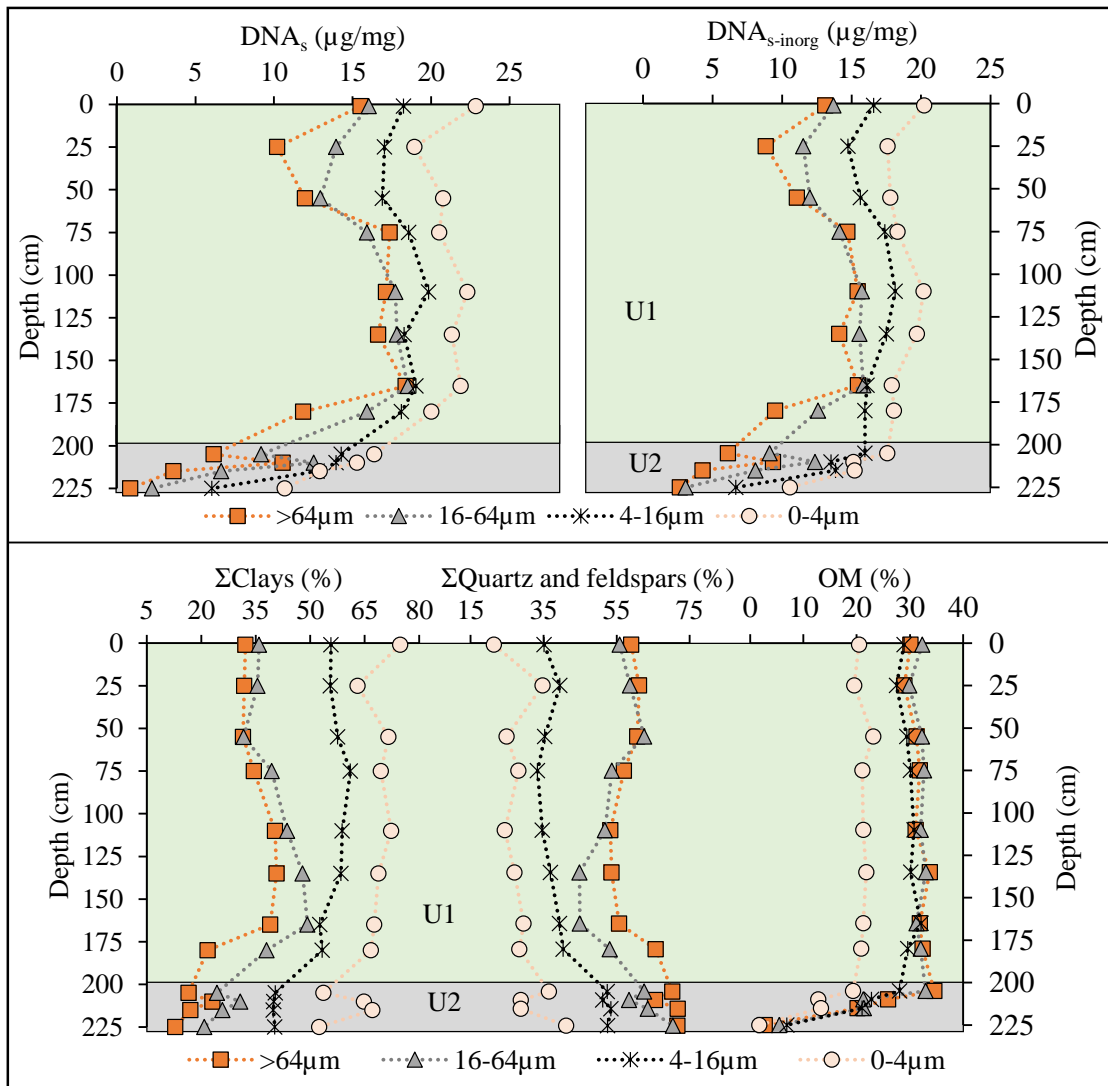
For example, the fraction $<4 \mu\text{m}$ is collected by taking the top 3 cm of the solution after keeping the suspension at rest for 31 min (i.e., $t=31$ minutes if the cut-off size $d=0.000004 \text{ m}$ and $h=0.03 \text{ m}$).

3. The sample is then centrifuged to collect the selected fraction (e.g., at 4,000 rpm for 30 min or higher speeds for less time). Discard the supernatant without disturbing the pellet.
4. DNA extraction is performed on the pellet which contains the fractions/particles of interest.

Some important notes to consider.

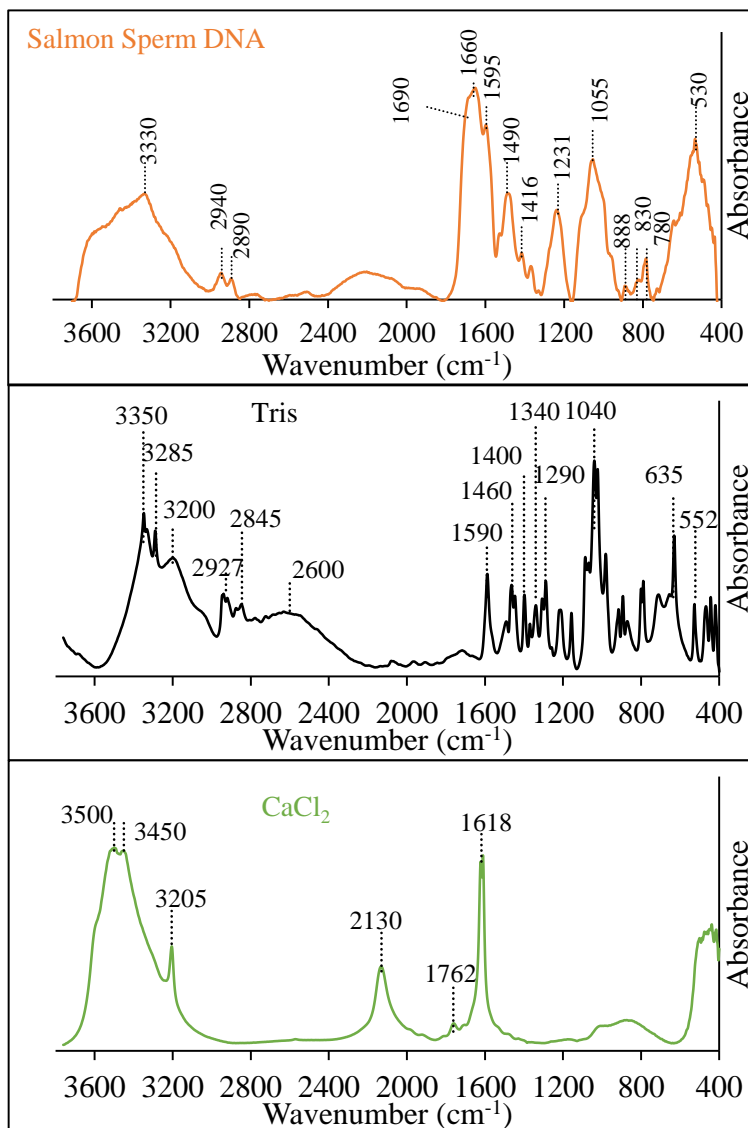
1. All steps are preferentially done under dark conditions.
2. Overnight shaking is optional; it helps in sample disaggregation.
3. Working with fresh samples (instead of previously frozen or freeze-dried) is preferred. Freezing and freeze-drying might introduce aggregates.
4. The mass of the sample used in size-fractionation depends on the mass of the material to be recovered. However, the concentration of the particles should be less than 5 g/L to avoid particle-particle interaction during sedimentation (which renders Stokes' law inapplicable).
5. Repeated collection of the desired fraction might be necessary to collect adequate masses for analysis. For example, after the collection of the suspension in "h" the first time, re-add sterile Milli-Q water, shake for a minute, let the container stand for sediment settling, and collect the fraction again.
6. The mass of the "dry" sample used for DNA extraction is preferably noted. This will lead to a better comparison between different samples. Reporting the DNA copies per dry mass would be optimum.
7. Any treatment, for disaggregation purposes, that leads to modification or destruction of DNA must be avoided. Never sonicate, heat, or add chemicals for disaggregation or removal of organic matter or carbonates (e.g., hydrochloric acid, acetic acid, hydrogen peroxide, or sodium hexametaphosphate).
8. The cut-off size depends on the abundance of clays and the recovery of adequate mass for analysis. If not enough sample is recovered for a certain size-fraction, even with more than one step "h" suspension collection, higher cut-off size is suggested. Cut-off size for clayey samples can easily be 4 μm , while it is expected to be higher for coarser particles (e.g., 20 μm).

Fig. A.1: Variation of DNA_s , $DNA_{s-inorg}$, $\Sigma Clays$ (chlorite+mica), $\Sigma Quartz$ and feldspars, and organic matter (OM) for different size fractions as a function of sediment depth



Clay minerals are predominantly present in the 0-4- μm size fraction. Nonetheless, clay minerals are also present in the coarse fractions due to mineral-mineral and organo-mineral aggregates.

Fig. A.2: Diffuse reflectance infrared Fourier transform (DRIFT) spectra for the initial compounds used in the DNA sorption experiment



References

- Cai, P., Huang, Q.Y., Zhang, X.W., 2006. Interactions of DNA with clay minerals and soil colloidal particles and protection against degradation by DNase. *Environ. Sci. Technol.* 40, 2971–2976. <https://doi.org/10.1021/es0522985>
- Lagaly, G., Dékány, I., 2013. Colloid clay science, in: Bergaya, F., Lagaly, G. (Eds.), *Handbook of Clay Science. Part A: Fundamentals*. Elsevier, pp. 243–381. <https://doi.org/10.1016/B978-0-08-098258-8.00010-9>
- Margenot, A., Calderón, F., Bowles, T., Parikh, S., Jackson, L., 2015. Soil organic matter functional group composition in relation to organic carbon, nitrogen, and phosphorus fractions in organically managed tomato fields. *Soil Sci. Soc. Am. J.* 79, 772–782. <https://doi.org/10.2136/sssaj2015.02.0070>
- Margenot, A.J., Calderón, F.J., Parikh, S.J., 2016. Limitations and Potential of Spectral Subtractions in Fourier-Transform Infrared Spectroscopy of Soil Samples. *Soil Sci. Soc. Am. J.* 80, 10–26. <https://doi.org/10.2136/sssaj2015.06.0228>
- Margenot, A.J., Parikh, S.J., Calderón, F.J., 2019. Improving infrared spectroscopy characterization of soil organic matter with spectral subtractions. *J. Vis. Exp.* 2019, 1–15. <https://doi.org/10.3791/57464>
- Mikutta, R., Kleber, M., Kaiser, K., Jahn, R., 2005. Review: organic matter removal from soils using hydrogen peroxide, sodium hypochlorite, and disodium peroxodisulfate. *Soil Sci. Soc. Am. J.* 69, 120. <https://doi.org/10.2136/sssaj2005.0120>
- Nguyen, T.T., Janik, L.J., Raupach, M., 1991. Diffuse reflectance infrared Fourier transform (DRIFT) spectroscopy in soil studies. *Soil Res.* 29, 49–67. <https://doi.org/10.1117/12.970790>
- Padilla, J.E., Calderón, F.J., Acosta-Martinez, V., Van Pelt, S., Gardner, T., Baddock, M., Zobeck, T.M., Noveron, J.C., 2014. Diffuse-reflectance mid-infrared spectroscopy reveals chemical differences in soil organic matter carried in different size wind eroded sediments. *Aeolian Res.* 15, 193–201. <https://doi.org/10.1016/j.aeolia.2014.06.003>
- Pedreira-Segade, U., Michot, L.J., Daniel, I., 2018. Effects of salinity on the adsorption of nucleotides onto phyllosilicates. *Phys. Chem. Chem. Phys.* 20, 1938–1952. <https://doi.org/10.1039/C7CP07004G>
- Smith, B.C., 1998. *Infrared spectral interpretation: a systematic approach*, 1st ed. CRC press.